IMPT

Leibniz
Universität Hannover

Institut für
Mikroproduktionstechnik
Prof. Dr.-Ing. Lutz Rissing

Evaluation and FMEA of Fabrication Techniques for Metallic Grating Couplers on Polymer Substrates with Low Glass Transition Temperatures

February-August 2016

Bachelor thesis

cand. Bachelor of Science Wejdene Gribaa

Matr.-Nr.: 2706120

First examiner: Dr.-Ing. Marc Wurz
Second examiner: Prof. Dr.-Ing. Ludger Overmeyer

Supervisor: Meriem Akin

This is an open access publication distributed under the terms of the Creative Commons Attribution License (CC BY) 3.0 Germany | https://creativecommons.org/licenses/by/3.0/de/deed.en).

Table of Contents

Table of Contents i
Table of Figures iv
1 Introduction 1
1.1 Motivation and Goal 1
1.2 Task Description 2
2 State of the Art 3
2.1 Current Optical Integrated Platforms 3
2.1.1 Glass 3
2.1.2 Lithium-niobate 3
2.1.3 III–V Semiconductors 3
2.1.4 Silicon-on-Insulator 4
2.1.5 Polymers 4
2.2 Polymers 5
2.2.1 Generalities on Polymers 5
2.2.1.1 Definition 5
2.2.1.2 General Classification 6
2.2.1.3 Common Properties 7
2.2.1.4 Cost of Polymer Materials 9
2.2.1.5 Some Important Thermoplastics 10
2.2.2 Polymers in Optics 11
2.2.2.1 General Requirements for Polymer Flexible Photonics 11
2.2.2.2 Optical Properties 12
2.2.2.3 Flexibility of Polymer Substrates 13
2.3 Vertical Coupling to Waveguide with Grating Couplers 17
2.3.1 Introduction 17
2.3.2 Definition of Diffraction Gratings 17
2.3.3 Common Types of Diffraction Gratings 19
2.3.4 Theory of Grating Couplers 20
2.3.4.1 Specifications of a Diffraction Grating 20
2.3.4.2 Bragg Equation 22

2.3.4.3 Coupling Angle 22
2.3.4.4 Detuned Gratings 23
2.3.4.5 Basic Geometry and Definition of Design Parameters 23
2.3.5 Materials of Metal Grating Couplers 24
2.4 Adhesion of Metallic Gratings to Polymers 25
2.4.1 Fundamentals of Adhesion 25
2.4.2 Joining Metals to Polymers 27
2.4.3 Adhesion Measurement Methods 28
2.4.3.1 Adhesion Main Theories 28
2.4.3.2 Mechanical Adhesion Tests 29
3 Processing of Grating Couplers 32
3.1 Basic Fabrication Methods 32
3.1.1 Mechanical Processing 32
3.1.2 Phase Masks 33
3.1.3 Photolithography 33
3.1.4 Electron-Beam Direct Write Lithography 34
3.1.5 Holographic Recording / Interference Lithography 34
3.1.6 Reactive Ion-Etching 35
3.1.7 Focused Ion-Beam Etching 35
3.2 Current Fabrication Schemes 36
3.2.1 Superplastic Nanoforming 36
3.2.2 Flip Chip Double Side Processing with a BCB Adhesive Layer 38
3.2.3 Nanoimprinting 41
3.2.4 Hot Embossing 44
3.2.5 Wet Etching 45
3.2.6 Mechanical Removal with Carbon Tubes 48
3.2.7 Stretchable Metallic Gratings 50
3.2.8 Laser & Dry Etching 52
3.2.9 Additive Nanopatterning 53
3.2.10 Melt and Mold Fabrication 55
3.2.11 Flip and Fuse 57
3.3 Overview Matrix 58

3.4 Evaluation and Results ... 64
4 Failure Mode and Effect Analysis of Procedures for the Fabrication of Metallic Gratings ... 67
4.1 Introduction ... 67
4.1.1 Origin of FMEA ... 67
4.1.2 Objectives of FMEA ... 67
4.1.3 Prerequisites ... 68
4.1.4 Legal Aspects of FMEA ... 68
4.1.5 Types of FMEA ... 68
4.1.5.1 Product FMEA ... 69
4.1.5.2 Process FMEA ... 69
4.1.6 Sequence of FMEA ... 69
4.1.7 Limitations of FMEA ... 70
4.1.8 The FMEA Procedure ... 70
4.2 Process-FMEA Application on the Flip and Fuse Technique ... 73
4.2.1 Sequence 1: Stamp Fabrication ... 73
4.2.2 Sequence 2: Flip & Fuse ... 78
4.2.3 Sequence 3: Separating by Bending ... 79
5 Conclusion ... 83
References ... 85

Table of Figures

Figure 1: PlanOS Concept [55]. 1
Figure 2: 150-nm Buried OXides (BOX) produced by low-dose oxygen implantation [9]. 4
Figure 3: The different polymer chemical structures: linear, branched and cross-linked [20]. 5
Figure 4: Temperature dependence of the E-modulus of polymers [10]. 6
Figure 5: Important thermal characteristics of standard polymers [63]. T_g is the glass transition temperature, T_m the melting temperature and HDT/A is the heat deflection temperature. 7
Figure 6: Price range per kilogram plastic granulate (Selection) in € for the year 2011 [10]. 9
Figure 7: Transmission curve of a 2 mm thick Plexiglas sheet (refractive index n=1.49) in air [23]. 12
Figure 8: Operation of a bent optical fiber [70]. 13
Figure 9: Photograph of a R2R machine for the large-scale fabrication of organic photovoltaic cells. The direction of the web movement is depicted alphabetically on the picture [21]. 15
Figure 10: Discrete processing [21]. 16
Figure 11: Inline processing [21]. 17
Figure 13: Reflected diffraction orders up to the 2nd mode by a diffraction grating of groove depth h and period d [6]. 18
Figure 12: Schematic illustration of an optical coupling device with input and output grating couplers. 18
Figure 14: An example of a volume grating with a period Λ, refractive indices n_1 and n_2, the slant of the periodic sections Φ and the wave vector K [18]. 19
Figure 15: Examples of surface relief gratings: (a) binary, (b) blazed, (c) sinusoidal [18]. 20
Figure 16: Diffraction orders in a trapezoidal grating with the grating vector K [18].. 20
Figure 17: Perfectly vertical coupling [46]. 22
Figure 18: Positively (right) and negatively (left) detuned gratings [46]. 23

Figure 19: Geometry and basic design parameters of a grating coupler [46]. 23
Figure 20: Micro-rough solid surface [14]. 29
Figure 21 : Diagram of pull-off test. The force F is applied at cylinders P_1 and P_2 with the force aligned through the center C of the substrate [40]. 30
Figure 22: Schematic illustration of a peeling test apparatus [40]. 31
Figure 23: Operation of a phase mask [18]. 33
Figure 24: Contact photo-lithography process for grating fabrication [18]. 34
Figure 25: Holographic recording of sinusoidal diffraction grating [18]. 35
Figure 26: Fabrication process of a diffraction grating die by lithography and Ni-electroforming processes [52]. 36
Figure 27: Configuration of one-shot exposure by an interference optical system [52]. 37
Figure 28: Schematic of the buried metal grating design [19]. 38
Figure 29: Schematic flow of metal-gratings fabrication and 3D view [19]. 39
Figure 30: (a) Second EBL step: cross section of the SiOx pattern. (b) FIB cross section of the metal grating (with 175 nm thick SiOx) before bonding. (c) Fourth EBL step: cross section of the bonding and top view SEM picture of the fabricated metal gratings [19]. 40
Figure 31: Schematic of the fabricated double resonance substrate [69]. 42
Figure 32: Schematic representation of the synthesis of Au NPs/MoO_3/Ag grating double resonance substrate [69]. 43
Figure 33: Embossing of the grating structure into the substrate [60]. 44
Figure 34: The proposed polymer-based surface grating coupler [62]. 46
Figure 35: The fabricating process of UV soft imprint lithography combined with wet etching to realize the proposed structure [62]. 47
Figure 36: SEM picture of the fabricated surface grating coupler with Si_3N_4 layer embedded between the core and under cladding layer [62]. 48
Figure 37: The physical model of the simulation with the metallic film structure and two open ended zigzag type CNTs [8]. 49
Figure 38: Snap shot from the simulation of the grating generating process [8], (No information was given about the color-scale). 49

Figure 39: Snap shot from the simulation of the grating formation [8], (No information was given about the color-scale). 50
Figure 40: Schematic illustration of the procedure used to fabricate stretchable metal gratings. 51
Figure 41: Schematic overview of the fabrication process [2]. 53
Figure 42: Schematic of procedures for nanotransfer printing (nTP) [33]. 55
Figure 43: The melt & mold fabrication of various devices (diffraction grating, well-plates and micro fluidic devices) using the same metal and different molds [31]...... 56
Figure 44: Molten metal being poured onto mold (example fabrication of a well-plate) [31]. 56
Figure 45: Donor fabrication process. 57
Figure 46: The DAMUK© model for the FMEA creation. 69
Figure 47: FMEA flow cycle. S, O and D are the Severity number, the Occurrence number and the Detectability number, respectively. RPN is the Risk Priority Number. 70
Figure 48: Schematic illustration of a rectangular grating pattern on the donor stamp. 74
Figure 49: Structures/ Layer order on the stamp (left) and on the receiver after transfer (right). 74
Figure 50: Schematic illustration of shape modification in an example of sinusoidal grating before (left) and after (right) load application 75
Figure 51: Pre-molding of the polyimide coating to fit in the shape of the metallic grating. 75
Figure 52: Fabrication model of a rectangular grating with a PI negative mold. 76
Figure 53: Two-step F&F processing. 76
Figure 54: Roughened surface after separation. 77
Figure 55: 3-Aminopropyltriethoxysilane embedded in the organic material PI to promote adhesion to the inorganic substrate. 77
Figure 56: Schematic illustration of the thermo-compressive load of the bonding tool for the pattern transfer. 78
Figure 57: Grating geometrical parameters: (left) before, (right) after fusion step. ... 79
Figure 58: Bending for separation of the rigid stamp and the polymer film. 80

Figure 59: (a) Strain after bending of ductile material, (b) Micro-crack after bending of brittle material 80
Figure 60: Stress-strain curve for ductile materials [35]. 81

1 Introduction

1.1 Motivation and Goal

The current work is under the umbrella of PlanOS, which is an ambitious collaborative research project, funded by the German Research Foundation and aiming to develop a next generation of optical sensor technology.

These sensors are using light to measure quantities such as temperature, strain or concentration of chemical compounds. They are manufactured on polymer-based thin sheets which are flexible, to allow more design and integration freedom than current rigid circuits. They are also compatible with large scale production for the different industrial applications such as medicine or packaging.

Figure 1 shows the concept of PlanOS project and its different sub units.

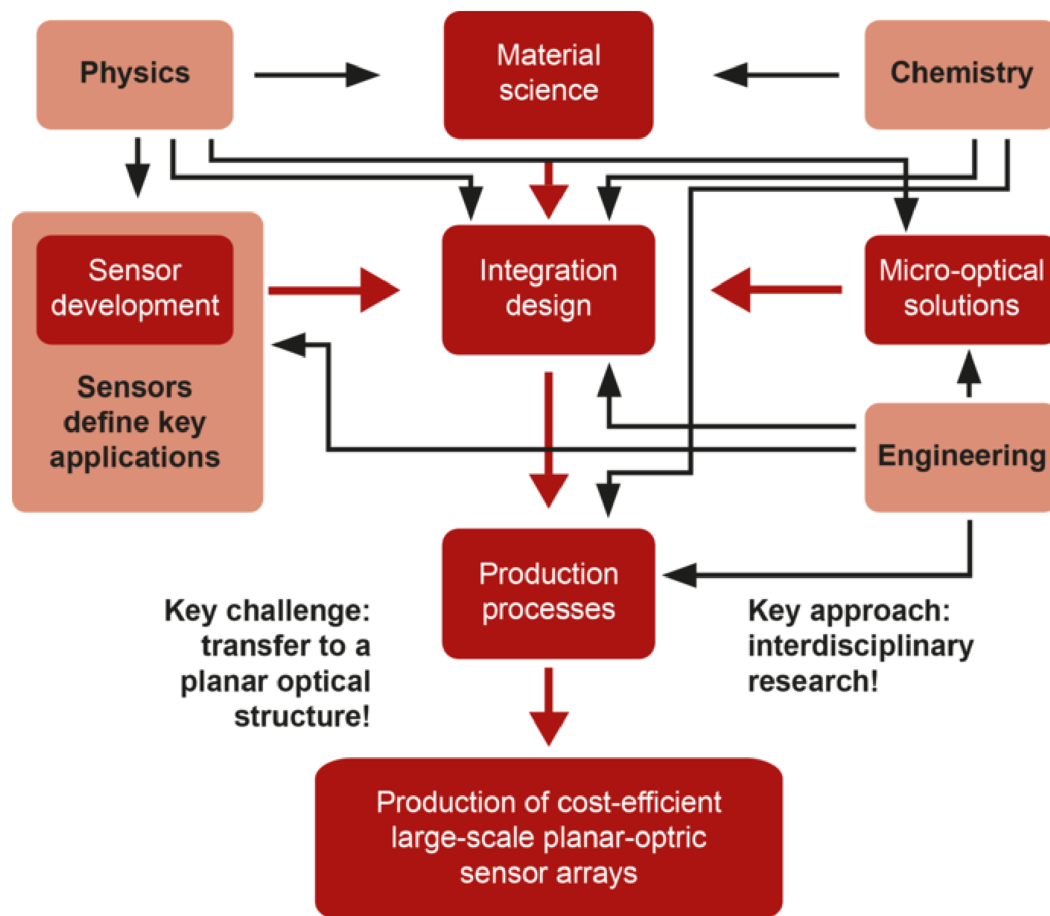

Figure 1: PlanOS Concept [55].

In order to guarantee a good interaction between all optical components of the sensor film; such as light sources, sensors and detectors; waveguides and coupling structures are used to guide the light inside the film and transfer it in and out of it.
These coupling structures are an important part of the project, since they are directly responsible for the efficiency of transmission and maximum performance of the sensor network. They are micro-optical structures, mainly composed of diffraction gratings.
The aim of this work is to help solve one of the main technical challenges in this area, which is the realization of such micro-structures on completely polymer-based substrates. The polymer substrates are needed because of their flexibility, low cost and mass production compatibility, but they are not very heat-resistant to allow processing of small structures under the high temperatures of the conventional fabrication methods.

1.2 Task Description

The main task is to analyze the state of the art of grating couplers production and low cost polymer substrates. Then to provide a recommendation of a new or adapted process for the production of metallic gratings on polymer sheets, based on a Failure Mode and Effect Analysis (FMEA).
In order to achieve that, this thesis is divided into four chapters.
After the first introductory chapter, the second section provides details about the state-of-the-art in optical technology platforms with focus on polymers and their main features for the aimed application, such as flexibility, low cost and roll to roll compatibility.
It defines then the diffraction gratings and their specifications and closes with the explanation of adhesion mechanisms of inorganic materials on polymer substrates.
The third chapter discusses processing of grating couplers. It introduces the basic fabrication methods and details a selection of current fabrication schemes found in literature with an assessment of their potential use for the desired application.
The last chapter is a FMEA analysis of the retained fabrication process, called Flip and Fuse, in order to check its capability to realize the grating structure.

2 State of the Art

Integrated optical chips are fabricated at present in a number of material systems. This chapter provides, in a first section, an overview of the currently most important ones, their applications, and some important platform parameters. Subsequently, the polymeric platform is discussed in detail; beginning with a presentation of the general definition, the principal features and characteristics, and closing with the main specifications in the field of large-scale integrated flexible photonics [38].

2.1 Current Optical Integrated Platforms

Optical chips are fabricated nowadays in III–V semiconductor material systems, with the possibility of monolithic integration of laser diodes, photodiodes, and passive components. They are also fabricated in different dielectric material systems that do not allow monolithic integration. Commonly used are lithium-niobate ($LiNbO_3$), glass-based material systems, silicon-on-insulator (SOI), and polymers [37].

2.1.1 Glass

Glass based technologies have good performance characteristics (esp. low losses at the fiber-chip coupling, and low propagation losses of waveguides). They operate in high end systems of optical communication technology, in the wavelength range 1.3-1.5 µm [37].

2.1.2 Lithium-niobate

Lithium-niobate ($LiNbO_3$) is a synthetic, ferroelectric crystal. It presents large acousto-optic and electro-optic coefficients and is used nowadays only for special components in high-end systems, such as Mach Zehnder modulators and acousto-optic filters. These devices can only be fabricated in this substrate material or with significantly lower quality in other material systems [37].

2.1.3 III–V Semiconductors

III–V semiconductors provide the monolithic integration of active and passive components on a single chip, such as semiconductor lasers and photodiodes. The InGaAsP is typically used in optical communication technology (in the 1.3-1.5 µm wavelength range). GaAlAs is mainly used in optical short-distance and

interconnection technology (in the 0.6-0.8 µm wavelength range). This material system is costly and thus limited in use in larger integrated optical circuits [37].

2.1.4 Silicon-on-Insulator

Silicon-on-insulator (SOI) is a technology for the fabrication of ultra dense electrical integrated circuits (ICs) that was initially developed by IBM. It is the practice of placing a thin layer of pure crystal silicon on top of an insulating material (like silicon oxide or sapphire) in order to speed up the performance of a microprocessor by reducing the capacitance of the transistors and making them operate faster and cooler [9]. The choice of insulator depends largely on intended application.
SiO_2-based SOI wafers can be produced by several methods. The SIMOX technique (Separation by IMplantation of OXygen) is widely used by IBM. It is based on injecting purified oxygen into the silicon wafer under a very high temperature. As a result, oxygen bonds with silicon and leads to the formation of thin layers of SiOx (see Figure 2).

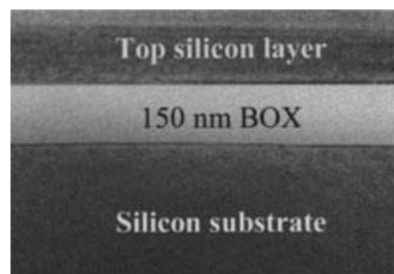

Figure 2: 150-nm Buried OXides (BOX) produced by low-dose oxygen implantation [9].

SOI wafers are very common in silicon photonics. The top silicon layer can be used to pattern optical waveguides and other passive optical components. To ensure total internal reflection of electromagnetic waves in the waveguide core, the silicon layer should be covered with a cladding material of a lower refractive index (usually air or silicon oxide).

2.1.5 Polymers

Polymers are mainly used for short and medium distance coupling and operate in the 0.6-0.8 µm wavelength range. They are not expensive and permit large area fabrication of integrated optical circuits [37].

2.2 Polymers

2.2.1 Generalities on Polymers

2.2.1.1 Definition

Polymers are macromolecules composed of a large number of atoms which are bonded together to form a chain structure. This structure has repeating elements called monomers [63].

The polymer chains can have different lengths and layouts (e.g. linear, branched or cross-linked; see Figure 3) and the molecule atoms are mainly carbon, oxygen, hydrogen and nitrogen. Inorganic components such as chlorine, fluorine or sulfur are also possible. Polymers are natural and synthetic products created through chemical reactions called polymerizations (e.g. condensation polymerization or chain-growth polymerization).

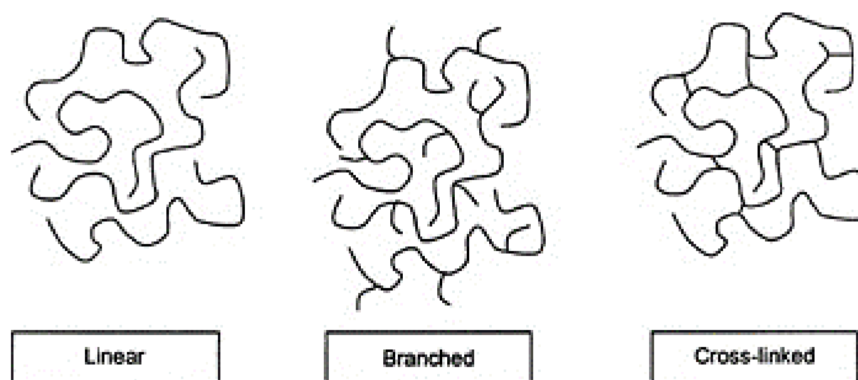

Figure 3: The different polymer chemical structures: linear, branched and cross-linked [20].

The chain length and ramifications in addition to the composition define together the main characteristics of polymers. Their thermal and photochemical stability is determined by the intermolecular covalent forces (van der Waals forces) and the chain entanglement [63].

Today, polymers exist with a wide range of properties, such as hardness, elasticity, glass transition temperature and chemical resistance. These characteristics can be determined by the choice of the polymer compounds, the fabrication process and by employed additives. In industry, they are very promising due to their lightness, high strength-to-weight ratio, ease of molding and low production cost.

2.2.1.2 General Classification

As mentioned above, polymers can be tailor-made to meet the requirements of the user through molecular design and synthesis [63]. The chemical structure of polymers has a strong influence on their physical properties, and affect their flow and morphology [49].

Based on the differences in the thermo-mechanical behavior, polymers can be divided into the following four groups according to DIN 7724 and [10, 53]:

- Thermoplastics are linear and slightly branched polymers that can soften or melt when heated. They can be re-processed and can either be hard or soft.
- Thermoplastic elastomers (TPE) are loosely cross linked, multiphase plastics, which soften or melt at a certain temperature. They exhibit advantages typical of both elastomeric and plastic polymers.
- Thermoset elastomers are amorphous, loosely cross linked polymers that behave elastic and are not meltable up to the decomposition temperature.
- Thermosets are highly cross linked polymers. They cannot be re-processed upon heat without permanent chemical degradation.

The following figures show the temperature dependence of the E-modulus of the different polymer groups and important temperature values for standard polymers.

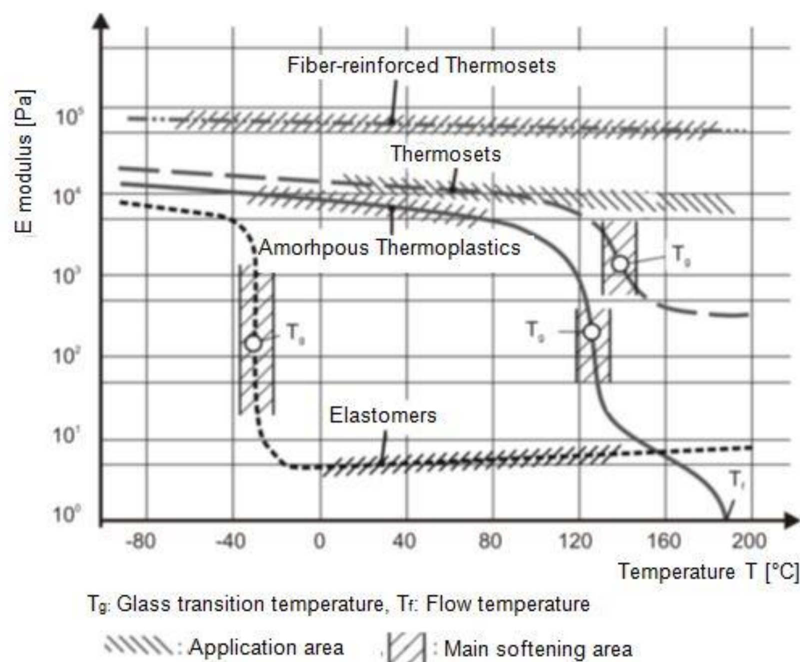

Figure 4: Temperature dependence of the E-modulus of polymers [10].

	T_g	T_m	HDT/A
PE-LD	−30	110	35
PE-HD	−100	135	50
PP	10	160	60
PBT	60	255	65
PVC	80		70
PA6 (kond.)	30	230	70
PS	90		80
PA66 (kond.)	40	260	80
PET	95	255	80
PMMA	110		95
ABS	−85/100		97
SAN	110		100
POM	−85	170	110
PA12	50	180	115
PC	145		125
PA11	50	185	145

Figure 5: Important thermal characteristics of standard polymers [63]. T_g is the glass transition temperature, T_m the melting temperature and HDT/A is the heat deflection temperature.

2.2.1.3 Common Properties

- Chemical resistance: This property is influenced by the nature of the applied chemicals to the polymer, their concentration, the temperature and the exposure time. In general, polymers have good chemical and physical resistance. Suitable additives, called stabilizers, can avoid the destructive chemical reactions of some substances with polymer materials to some extent. Thermoplastics generally exhibit high resistance to acids and alkalis, and thermosets to organic solvents. Internal tensions and mechanical stress caused through the molding have also impact on the chemical resistance. Chemicals can affect the strength, flexibility, surface appearance, color, dimensions or weight of plastics [3].
- Thermal conductivity: Plastics are poor heat conductors. High thermal conductivity may be important for the cooling of current-load circuits [66].
- Thermal resistance: The behavior and properties of polymers (mechanical, electric and chemical) are far more affected by temperature than metals. While for temperature sensitive polymers, the maximum operating temperature is between 90-150 °C, more heat resistant types, such as polyimide PI, can be processed with temperatures of 200-350 °C. The duration of the temperature effect is in all

cases decisive. Very low temperatures (below 0 °C) have hardly any changes on the performance of thermosets, while thermoplastics may harden to the point of brittleness. Very high temperatures, often starting at about 300 °C, lead in all polymers to chemical decomposition [3].

- Electrical properties: Polymers exhibit excellent insulating resistance. They do not conduct electricity, because there are no free electrons in their molecular structure. The dielectric strength depends on the composition of the polymer material and to a large extent on the material thickness. It is significantly higher with thin films than with thicker plates because of their more homogeneous molecular cohesion [3].
- Optical properties: A valuable addition to the choice of materials for specific applications is the fact that amorphous polymers are transparent. The transparency in many polymer types can vary depending on the additives in the chemical formula from clear to slightly translucent. Thus, they supplement the usual types of glass with better mechanical properties (such as impact strength and resistance to breaking and to splintering) and, in special cases, with their improved optical properties. Requirement for glass clarity is the disorder of the amorphous state. Transparent is a material which is optically homogeneous, i.e., it has the same refractive index in all locations regardless of the direction (see also example of Polymethylmetacrylate (PMMA) under 2.2.2.2.1). Additives that have a different refractive index may reduce the transparency of the polymer or even raise it [3]. A classification of polymers based on the color is limited, because most plastics can be transparent or opaque dyed in all colors. Phenolic resins (PF) are, for instance, always dark colored because of their yellowish brown natural color. PMMA is particularly distinguished with a good transparency and brilliant surface gloss (see more details under 2.2.2.2.1). Crystal clear, unless opaque dyed, are mainly polystyrene (PS), polycarbonate (PC) and the thermosetting unsaturated polyester (UP). Not entirely clear, translucent is Low Density Polyethylene (LDPE) and milky white is High Density Polyethylene (HDPE).
- Mechanical properties: Rigidity, stress-strain and impact strength of amorphous thermoplastics are mainly determined by the intermolecular bonds between the

chains, not by the covalent bonds within them. These intermolecular bonds are, depending on the chemical composition, van der Waals, dipole, or hydrogen bonds. The different strengths of these bonds cause the wide spectrum of mechanical properties of polymers. In addition, the geometry of the molecules is important because it determines whether they can move against each other especially in a plastic deformation [51].

- Physical properties: The glass transition temperature, T_g, is a critical temperature that is defined as the temperature over which the glass transition happens: the polymer transforms from a brittle and hard state (below T_g) to a viscous liquid and rubber-like state (above T_g). It is usually lower than the melting temperature, which is when the polymer changes from a rubbery state to a liquid [49].

2.2.1.4 Cost of Polymer Materials

The price of polymers is strongly dependent on the frequency of occurrence of the raw materials and the difficulty of obtaining them. The following table (see Figure 6) shows the price range in € for a selection of polymer materials [10]:

Polymers / Metals	Euro €/t	Polymers / Metals	Euro €/t
PE-HD	1,32–1,49	PA11	7,50–11,50*
PP	1,45–1,67	PA12	7,50–11,50 *
PS	1,75–1,96	PA 6	2,77–3,30
PVC	1,23–1,32	PA 6GF	3,11–3,40
		PA 6.6	3,73–3,90
ABS	2,10–2,85	PBT	3,35–3,68
PC	3,37–4,03	POM	2,91–3,42
PMMA	2,97–3,22	PET	1,55–1,75
PEI	10,0 –17,00*	PPS	3,00–10,50*
SAN	1,50–2,50*	PTFE	ca. 12,50*
SB	0,90–1,50*	LCP	ca. 50,00*
PSU	13,50*	PEEK	ca. 60,00*
For comparison			
St 37	0,30–0,50*	TPO	2,50–5,00*
Al	0,70–1,00*	TPU	3,75–6,25*
Mg	1,50–2,00*	UP	2,60–5,00*
Ti	4,00–5,00*	PF (vorvernetzt)	1,00–3,00*
C-Gewebe	80,00–120,00*	EP	4,00–10,00*

* Price range per kilogram plastic granulate in € for the year 2007

Figure 6: Price range per kilogram plastic granulate (Selection) in € for the year 2011 [10].

2.2.1.5 Some Important Thermoplastics

- Polyethylene terephthalate (PET) is a semi-crystalline, polar, hard and tough plastic with low creep and high abrasion resistance. It is insoluble in organic solvents. Moldings of PET have high dimensional stability and creep rupture strength with good sliding and wear properties. It is used for beverage bottles and heat-stressed household electrical appliances, rolls of all kinds, chains, springs, screws, and bearings [10].
- Polycarbonate (PC) is a crystal clear, well dyeable plastic with high weather resistance, usable at 120-140 °C, tough and hard with low creep tendency. PC has low water absorption, thus very good electrical insulation properties. PC is not resistant to benzene, organic solvents and strong acids. PC is also vulnerable to stress fractures; however, this can be improved by fiber reinforcement. PC finds application in components of precision and electrical engineering such as housing, connectors and CD discs. It is also used for covers of traffic lights and car lights, lenses and spectacle lenses and extruded sheets as plates for greenhouses [10].
- Thermoplastic elastomers (TPE) have rubberlike properties, but are thermo-plastically processed; because they do not form insoluble chemical cross-links, but rather present mechanical linking by entanglement of harder immovable moieties [10].
- Polymethylmethacrylat (PMMA): PMMA is a hard and relatively more brittle thermoplastic. It is prepared by radical polymerization and is commercially known as Plexiglas, Degalan and Acrylite®. PMMA is weather resistant and can be equipped with a scratch resistant surface. Because of its transparency, this polymer is used particularly and frequently in light transmission applications (see 2.2.2.2.1 for details). Typical applications include lenses and watch glasses, light conducting fibers, optical storage devices, flat panel displays, aircraft glazing, traffic signs, sinks, bathtubs, dental fillings and dentures [26].

2.2.2 Polymers in Optics

2.2.2.1 General Requirements for Polymer Flexible Photonics

For the choice of flexible polymer substrates in photonics, many requirements have to be considered [66]. Mainly: transparency, flexibility and rollability, low-cost, resistance to chemical attack, dimensional stability under thermal cycling and low permeability to water and oxygen [54].

Plastic films are very appealing substrate materials for flexible photonics due to their low cost and mechanical and optical properties. Semi-crystalline and biaxially oriented polymers are less favorable for the implementation into a roll-to-roll (R2R) processing format. This mechanical limitation is related to the high Young's Modulus of the plastic film, i.e. a considerable stiffness (Compatibility to R2R processing is subject of section 2.2.2.3.2) [54].

Substrates for flexible photonics must also be able to resist the working temperature of the coating deposition process [54]. The deposition substrate and the coating material can be optimized to the fabrication machine or vise versa. In the case of low thermal budget, the highest processing temperature (T_{max}) should not exceed the glass transition temperature (T_g) of the specific polymer material. Heating above this characteristic value causes changes of the physical and mechanical properties of the substrate film. As mentioned above (under 2.2.1.3), at temperatures near the $T_{g,}$ the polymer shows a liquid-like flow behavior and a significant decrease of the material's dimensional stability under tension. Semi-crystalline materials have also the natural tendency to shrink upon cooling: The microstructure of the polymer changes during device fabrication from biaxially oriented chains along the direction of film rolling to more ordered crystallites upon cooling after coating deposition [54]. Even small rates of shrinkage may cause cracking in top layers of the coating material (e.g. Indium Tin Oxide ITO [54]) and damage the properties of the flexible product. Pre-annealing of the film and minimizing the web tension can neutralize the effects of the shrinkage factor and improve the structural stability of the material [54].

The thermal expansion coefficients (CTE) of the thin film layers and the deposition substrate are also an important factor. Large discrepancies are detrimental and can lead to stress and crack formation [42].

In addition, the substrate should not release contaminants and should be inert against process chemicals [66].

2.2.2.2 Optical Properties

2.2.2.2.1 Light Transmittance

When light comes in contact with the surface of an object, it can either be reflected or propagates through the material. In the case of a transparent or a semi-transparent material, the redirected light can be transmitted, refracted or absorbed; where transmission of light simply means when light waves propagate through a sample without being absorbed. The transmittance of a material is related to the fraction of the incident light that has been transmitted, i.e., that propagated through the material from one side to the other.

A colorless PMMA sheet has the transparency of the optical glass, a total light transmission of 92%, and average haze values of only 1%. When a light beam encounters colorless Plexiglas sheet perpendicular to its surface, most of it is transmitted, some is reflected at both the top and bottom surfaces (about 8%), and a negligible fraction is absorbed (see Figure 7) [23].

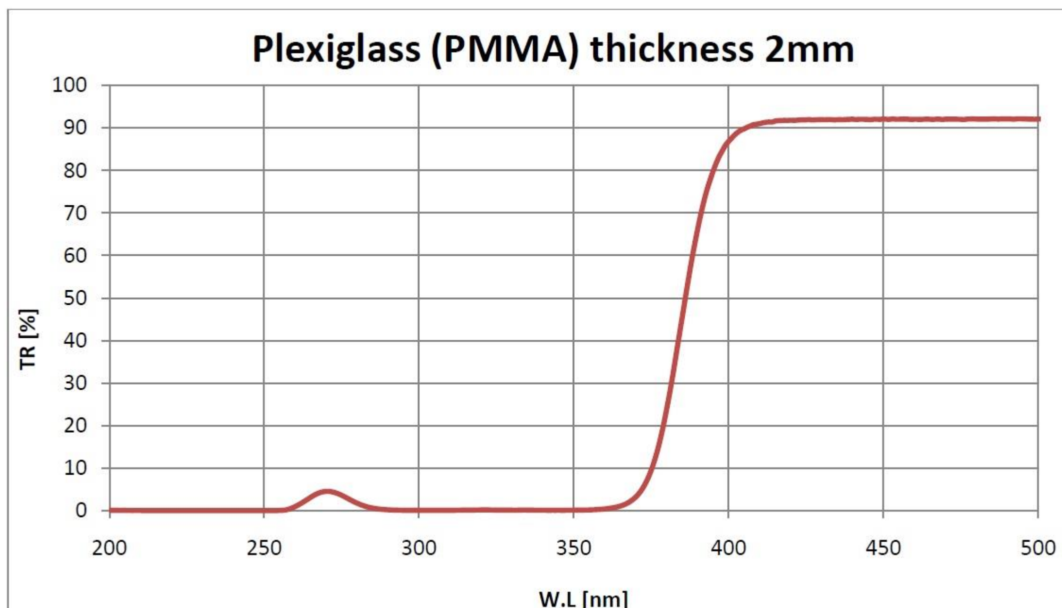

Figure 7: Transmission curve of a 2 mm thick Plexiglas sheet (refractive index n=1.49) in air [23].

The transmittance of an optical medium depends on its refractive index and on the angle of incidence respective to the normal of the light beam. The light absorbance is dependent, inter alia, on the thickness of the object. PMMA sheets of thicknesses up to 25.4 mm, show very low absorbance rates of less than 0.5% [23]. The curve on Figure 7 shows three main regions: Transmission above wavelengths of 400 nm, dominance of the bulk absorption below 400 nm and no light transmission below 360 nm.

2.2.2.2.2 Optical Inhomogeneities

- Effects of moisture absorption: It can modify the optical geometry of a component and thus its optical properties (such as refractive index) or introduce optical inhomogeneities especially in moisture-sensitive materials like acrylics [5, 7, 29].
- Effects of bending of the polymer film: In the fiber regime, bending of the optical device results in coupling losses as depicted in Figure 8 [57].

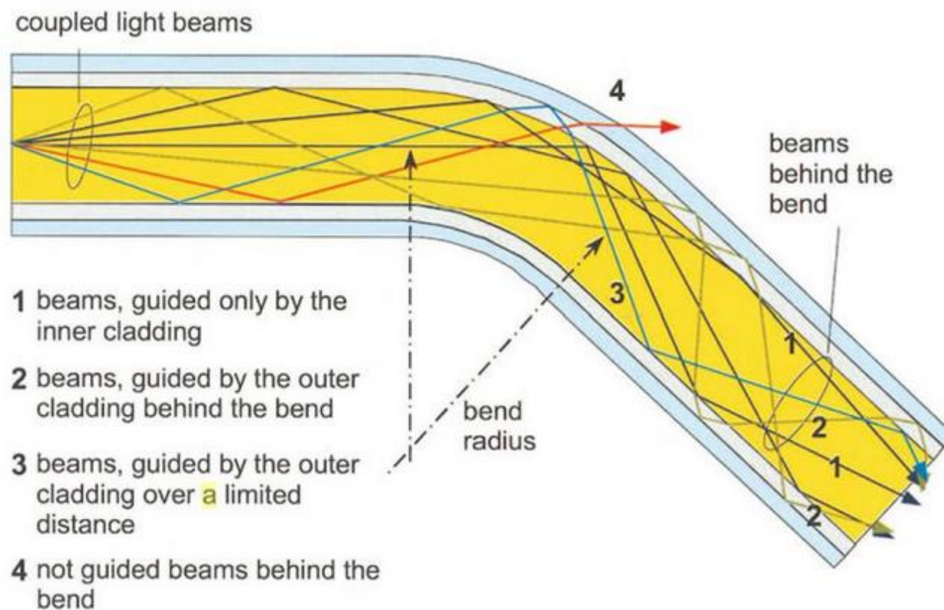

Figure 8: Operation of a bent optical fiber [70].

2.2.2.3 Flexibility of Polymer Substrates

Substrates or circuit boards are commonly classified according to their flexibility in three groups: rigid, flexible and rigid-flex printed circuit boards (PCBs). Rigid substrates are mainly made of laminates. These consist of an insulating carrier

material (such as paper, ceramics and glass tissue) and a binder (such as phenolic resin, polyimide and polyester). Flexible circuit boards generally consist of polymers. Rigid-flex PCBs are a combination of the two other substrate types [13].

2.2.2.3.1 Definition of Flexible Substrates

Flexible substrates may be defined as bendable, conformally shaped, elastic, lightweight, non-breakable or roll-to-roll manufacturable [66].

The integrated flexible structure must endure a certain bending load without the loss of its function. To make such flexible devices, the completed circuits are either bonded to a flexible substrate or directly fabricated on the substrate [66].

The first approach provides high-performance devices on flexible substrates at the expense of the surface area coverage and the cost. The second approach aims, in contrast, at manufacturing large-area and low cost flexible devices.

The flexibility of the substrate is given by its flexural rigidity, defined as [66]:

$$D = Et^3/12(1-\upsilon^2),$$

where E is Young's modulus, t is the thickness of the substrate, and υ is its Poisson ratio. According to its degree of flexibility, a sample can be bendable or rollable, permanently shaped or elastically stretchable.

For flexible applications, three types of substrate materials are available: metals, organic polymers and flexible glass. In the case of polymers, the following materials are of high interest for flexible devices [66]:

- The thermoplastic semi-crystalline polymers: polyethylene terephthalate (PET) and polyethylene naphthalate (PEN),
- The thermoplastic non-crystalline polymers: polycarbonate (PC) and polyethersulphone (PES), and
- High-T_g materials: polyarylates (PAR), polycyclicolefin (PCO), and polyimide (PI).

2.2.2.3.2 Roll-to-Roll Compatibility of Polymer Films

Polymer photonic devices are of growing interest for large scale industry. Conventional fabrication methods used to create these devices, such as photolithography, electron-beam lithography and reactive ion-etching (see 3.1), are costly, time consuming and sometimes very elaborated [27]. To fulfill current

industrial needs, solutions are required. In [56] for instance, a novel fabrication process to overcome the hindrances of the listed methods, achieving high throughput and lower costs with the flexibility of the substrate material choice, is presented. It consists in fabricating a photonic device combining imprinting and ink-jet printing methods.

The roll-to-roll (R2R) manufacturing concept is very favored for the industrial scale applications, thanks to its very high throughput compared to other manufacturing processes. The fabrication process is also continuous, which reduces the time investment in lifting and returning the imprint roller [21], along with the additional requirements for the adjustment of position and alignment. The fabrication can be implemented at ambient conditions (no vacuum, no clean-room and no evaporation) with printing and coating methods and, thus, ensuring further decrease in fabrication costs. Figure 9 shows a machine for full R2R processes.

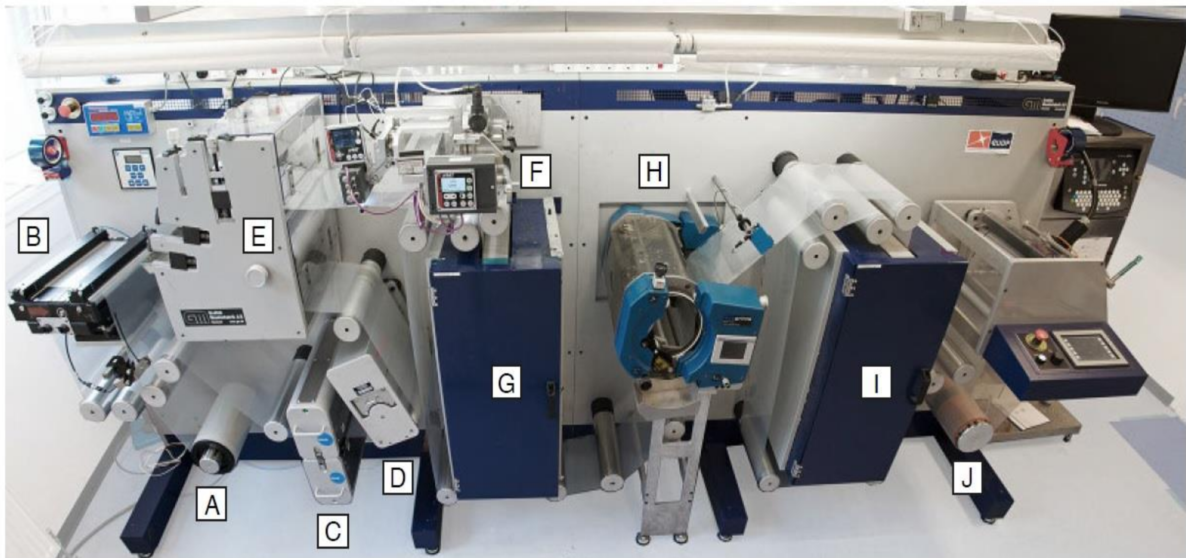

Figure 9: Photograph of a R2R machine for the large-scale fabrication of organic photovoltaic cells. The direction of the web movement is depicted alphabetically on the picture [21].

The processing units that can be implemented in a R2R setup range from the cleaning and preparation until the packaging stage. Different coating and printing processes can be used: blade coating, spray coating, slot die coating, screen printing, flexographic printing, gravure printing and inkjet printing.

Cleaning modules include contact and contactless cleaning as well as suction. They are used prior to printing to get rid of any impurity from the surface of the roll.

Pre-treatments of the substrate surface such as corona or plasma are other important processing steps. They alter the surface properties (especially the surface energy) and thus enhance the wetting capability and promote the adhesion of the imprinting material (such as silver) to the substrate (see chapter 2.4).
Dryers and annealing stations are used after imprinting/coating to dry the wet ink layer before meeting the next roller. UV-curing, microwave drying or thermo drying with hot air ovens are commonly used in this step. The maximum drying temperature is limited by the substrate material (e.g. 130-140 °C for PET) and the drying time is dependent on the web speed and the dryer length.
Processing modules based on laser energy have also been developed for R2R fabrication strategies, and comprise so-called scanning and fixed optic processes.
The last processing units of a R2R setup are the packaging stations for the delivery of the final functional device. They include encapsulation, cutting reel and cutting sheet stations.
R2R fabrication can be performed in two different fabrication scenarios or most commonly in a combination of both of them. Functional layers of multilayer devices can be printed or coated according to a discrete or to an inline processing method, or both. The process parameters have to be chosen such as to obtain a final product with the specific design features. Drying time or temperature, ink material, speed and layer thickness are some of the most important set up parameters. Figure 10 and Figure 11 show, respectively, a simplified schematic illustration of a discrete and an inline R2R fabrication strategy.

a) Discrete processing:

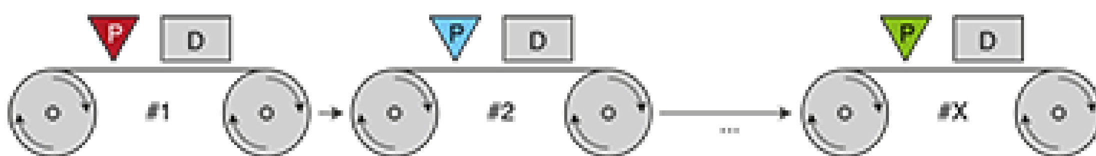

Figure 10: Discrete processing [21].

The discrete method is preferred for research aims. The functional layers are individually processed and the process parameters (fabrication method, ink, speed, drying) are refined for each layer requirements.

b) Inline processing:

Figure 11: Inline processing [21].

Ideally, all of the layers would be processed in the same machine in a single process run. The different processing stations are optimized in order and length for the definite device. An obvious disadvantage of this method is that, if it fails in processing a layer, the complete device can be defect. The inline processing has the merits of moderating bending stress, reducing handling and accelerating the workflow [21, 22].

2.3 Vertical Coupling to Waveguide with Grating Couplers

2.3.1 Introduction

Diffraction gratings are very important optical devices that have been used since the 18th century to analyze the spectrum of light. They find use in many fields of science like chemistry, physics, astronomy and biology [32]. With the development of science, diffraction gratings are nowadays also used for other applications, such as optical interconnects for computer systems, integrated optical devices, and optical communications [6]. In this thesis, the device of interest is the diffractive grating coupler, used in integrated optical chips to couple light from a light source to a waveguide or from a waveguide upwards to a light detector. This chapter is dedicated to this purpose, presenting an overview of diffraction grating. A general definition, common types of diffraction gratings and the diffraction equation are given in the following sections.

2.3.2 Definition of Diffraction Gratings

Diffraction gratings are optical components with a periodically modulated surface used for the efficient coupling of light from a free space source to a waveguide. A coupler can also be used to diffract light from a waveguide into a free space detector [58]. The basic structure of such an optical device is illustrated in Figure 12:

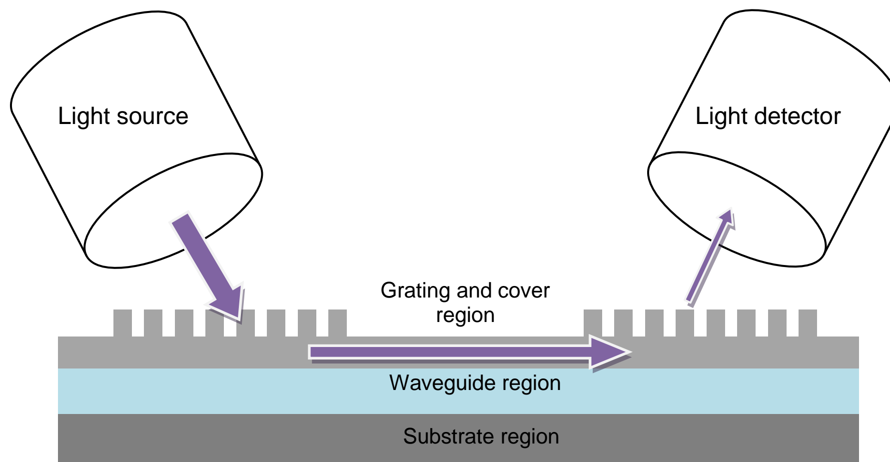

Figure 12: Schematic illustration of an optical coupling device with input and output grating couplers.

Diffraction gratings interact with the incident light to redirect it by reflection or transmission into specific diffractive orders at discrete angles [32] (see Figure 13). This effect is explained by the diffraction phenomenon, which occurs when a light wave encounters the surface of a periodic structure or goes through a medium with a varying refractive index [61]. This results in a diffraction pattern consisting of a periodic modification of the amplitude or the phase of the redirected wave. An example for this is the rainbow diffraction spectrum obtained when a diffractive grating is illuminated with a continuous white light.

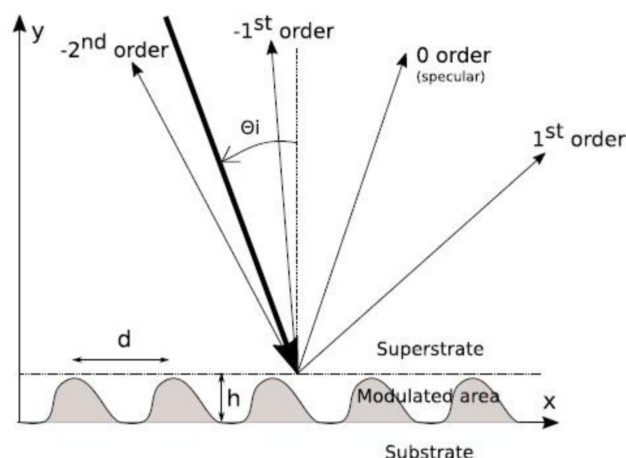

Figure 13: Reflected diffraction orders up to the 2nd mode by a diffraction grating of groove depth h and period d [6].

Gratings are highly dispersive and the angles of the diffractive orders strongly depend on the wavelength of the incident light. The orientation of the diffraction orders can be determined through the diffraction equation presented in 2.3.4.2.

2.3.3 Common Types of Diffraction Gratings

The very first diffraction gratings fabricated were a grid of periodic slits. Diffraction gratings are generally classified under two categories: amplitude gratings and phase gratings [32].

1) Amplitude gratings are an array of apertures that only give a spatial alteration of the amplitude of the transmitted wave. They either periodically block the beam, or attenuate it slightly [18].
2) A phase grating consists of a periodic structure of multiple corrugations with alternating index of refraction. These gratings give a spatial alteration of the phase of the diffracted beam and are classified in volume gratings and surface relief gratings:
   a) A volume grating is characterized by a flat surface profile. It is made of repeating periodic fragments with alternating indices of refraction. The direction of periodicity in such a grating can also be oblique to the substrate surface (see Figure 14). This feature makes volume gratings very important for the use in optical interconnect systems, since they can achieve with this flexible configuration efficiencies of almost 100%. They can be easily fabricated by holographic recording (see section 3.1.5).

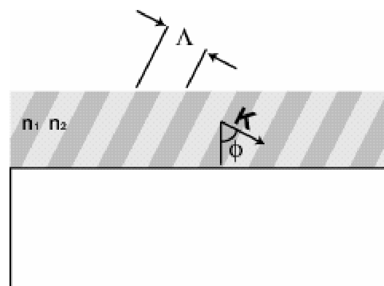

Figure 14: An example of a volume grating with a period Λ, refractive indices n_1 and n_2, the slant of the periodic sections Φ and the wave vector K [18].

   b) Surface relief gratings have, in contrast to volume gratings, a periodically changing topography with two alternating indices of refraction from the grating substrate and the cladding medium. Figure 15 shows the three important surface relief gratings. The binary grating consists of a simple periodic rectangular structure and can be easily manufactured by photolithography (see section 3.1.3). The sinusoidal grating is fabricated by holographic

recording or recording the interference of two uniform beams (see section 3.1.5). The blazed grating is manufactured by mechanical scribing (see 3.1.1) with limitations for small periods, and is generally designed to have only one dispersive propagating diffractive order (other than the 0th order) to maximize the diffracted efficiency. This is achieved by choosing the appropriate design parameters that appear in the diffraction equation, such as period, angle of incidence and incident frequency (see Equation 2).

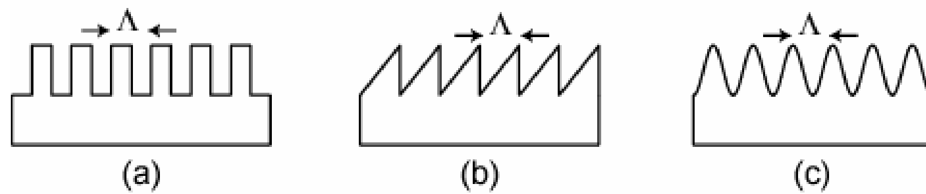

Figure 15: Examples of surface relief gratings: (a) binary, (b) blazed, (c) sinusoidal [18].

2.3.4 Theory of Grating Couplers

2.3.4.1 Specifications of a Diffraction Grating

A diffraction grating is characterized by its grating vector K, which is defined by having the magnitude $\mathrm{K} = \frac{2\pi}{\Lambda}$, where Λ is the period of the grating, and points in the direction of periodicity (see Figure 16) [58].

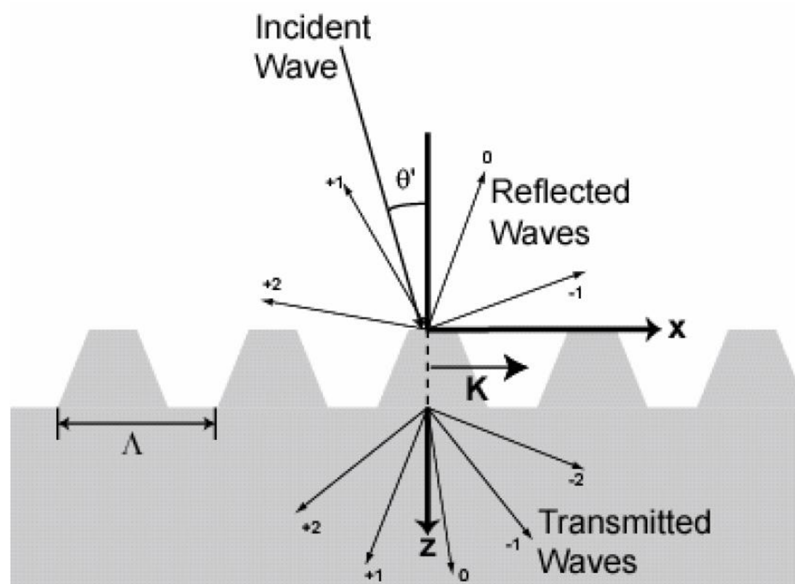

Figure 16: Diffraction orders in a trapezoidal grating with the grating vector K [18].

The resulting wave vectors upon diffraction by the grating can be described through the Floquet condition, where discrete multiples of the grating vector are added to the incident wave vector according to Equation 1 [6]:

$$k_m = k_{in} - m\mathrm{K}, \qquad \textbf{Equation 1}$$

with $m = 0 \pm 1 \pm 2 \ldots \pm \infty$ an integer denoting the number of the diffracted order, k_{in} the wave vector of the incident beam, and k_m is the wave vector of the mth diffracted order.

The Floquet condition gives an infinite set of diffracted orders. “However, only certain of those orders can exist physically” [6]. The possible propagative orders (including the reflective specular order) are obtained when the magnitude of k_m is smaller than or equal to the wave-number $2\pi n_i/\lambda$. Similarly, a diffractive order is evanescent if the magnitude of k_m is larger than this wave-number. The finite number of the diffractive orders and the diffraction angles for the reflected and transmitted rays can be calculated from the diffraction equation (see Equation 2). According to this equation, the number of orders for a given wavelength and angle of incidence depends only on the period of the grating and the material parameters of the cladding and diffraction medium.

The diffraction grating is also characterized by its efficiency, defined by the ratio of energy in the diffracted orders relative to the total incident energy [58]. The efficiency of a diffraction grating significantly depends on the groove shape and structure of the grating (including the grating period, the corrugation depth, the filling factor and the thickness of the top layer) [32]. Adding to that, the coupling efficiency depends on the dielectric permittivities/ magnetic permeabilities, and is highly sensitive to the incident field polarization [6]. The two possible polarizations for the propagation of fields in a medium are the transverse electric (TE) and the transverse magnetic (TM) polarizations. In the TE polarization, the electric field is perpendicular to the plane of incidence and in the TM polarization, it is the magnetic field that is normal to this plane [6].

2.3.4.2 Bragg Equation

The general form of the diffraction equation that describes the operation of a grating can be written as follows [32]:

$$n_m \sin\theta_m + n_{in} \sin\theta_{in} = {}^{m\lambda}/_{\Lambda}, \quad \textbf{Equation 2}$$

where Λ denotes the grating period, λ the wavelength of the incident light, θ_m the angle of the diffracted wave measured to the normal, θ_{in} the incidence coupling angle, n_m and n_{in} are the refractive index of the diffraction and incidence region respectively and m is an integer denoting the diffraction order.

As explained earlier, the diffraction equation describes only the relation between the wave vectors of the incident and diffracted beams for a particular coupling angle, and does not give the efficiency of the used structure.

2.3.4.3 Coupling Angle

Vertical coupling of the fiber to the grating results in great efficiency losses since the incident power will be divided and coupled horizontally in both directions in the waveguide (see Figure 17) [58]. This can be avoided by using an asymmetrical grating or by coupling the fiber with a certain angle (generally 8 to 10 degrees).

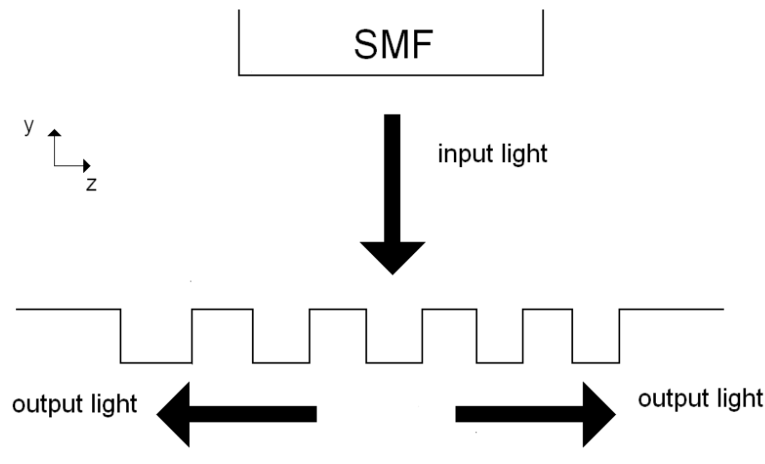

Figure 17: Perfectly vertical coupling [46].

2.3.4.4 Detuned Gratings

The coupling angle can be either positive or negative. The grating is then called detuned and the coupling schemes are shown in Figure 18.

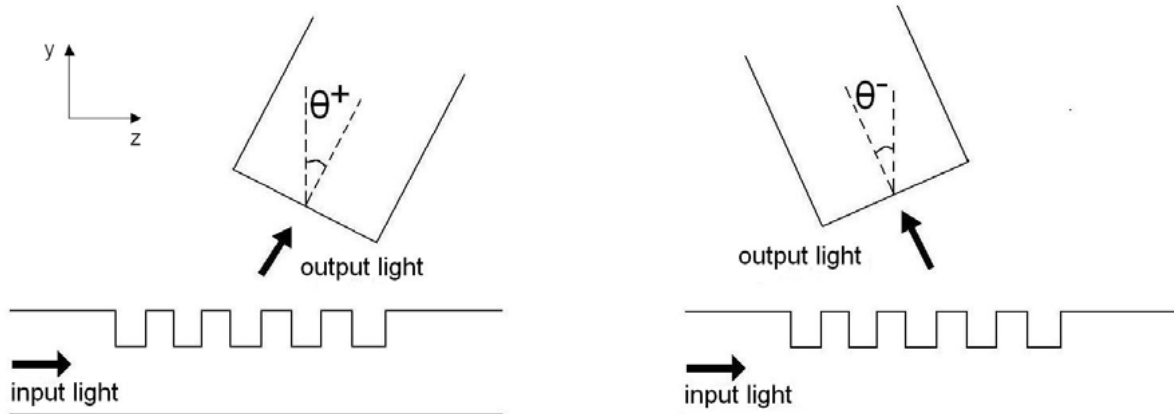

Figure 18: Positively (right) and negatively (left) detuned gratings [46].

The setup of positively detuned gratings is preferred for design and simulation.

2.3.4.5 Basic Geometry and Definition of Design Parameters

Diffraction gratings with periods up to 1 µm can be utilized for optical applications in the visible wavelength regime [68], where the wavelength ranges between approximately 400 to 700 nm.

The basic structure and the design parameters of a grating coupler are illustrated in Figure 19.

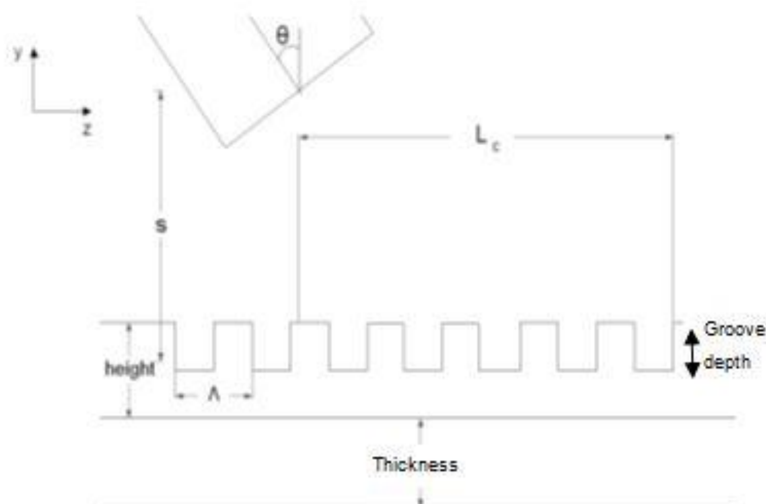

Figure 19: Geometry and basic design parameters of a grating coupler [46].

The structural parameters depicted in Figure 19 are defined as follows:

- Groove depth (gd): the depth of the grating slot
- Height: the height of the guiding core
- Thickness: the thickness of the under cladding material
- θ: the incidence angle of the light
- s the coupling length in the y direction; the vertical distance between the light source center and the waveguide centre.
- L_c the coupling length in the z direction; the horizontal distance between the light source and the beginning of the grating that provides maximum output power. L_c can be calculated according to Equation 3:

$$L_c = {}^{w_0}/_{1.37\ \cos\theta_{in}}, \qquad \textbf{Equation 3}$$

in which w_0 stands for half of the width of the incident beam, and θ_{in} for the incidence angle.

- Filling factor (ff): the relation between the widths of the cleaved and the non-cleaved sections
- Effective index (n_{eff}): the average effective index is calculated by means of Equation 4:

$$n_{eff} = (1 - ff).n_{eff_gap} + ff.n_{eff_tooth} \qquad \textbf{Equation 4}$$

with n_{eff_gap} and n_{eff_tooth} are found using the conventional Effective Index Method explained in detail in [46].

- Grating period Λ: its theoretical value is obtained from the grating equation:

$$\Lambda_{theo} = \frac{\lambda_0}{n_{eff} - n_{in}\sin\theta}, \qquad \textbf{Equation 5}$$

with n_{eff} the refractive index of the guided mode and n_{in} the refractive index of the cladding medium (generally air with n_{air}= 1).

2.3.5 Materials of Metal Grating Couplers

The use of metal for the fabrication of grating couplers provides very good performances and efficiencies due to the natural strong dispersion properties of the material [43]. In addition, the periodic structuring of the surface of the metal strongly

modifies the optical properties of the metal and can even lead to perfect light reflection or transmission [6]. This is explained by the high contrast between the refractive indices of the metallic grooves and the surrounding medium.

Diffraction gratings can be manufactured out of many metallic materials depending on the wanted efficiency or the application environment. Very common metals are titanium (Ti), copper (Cu), gold (Au), silver (Ag) and aluminum (Al) [16]. Chromium (Cr), widely used for photolithography masks [20], has also been used in [36] to create sputtered metallic gratings with a period of 200 nm.

Silver and gold are favorites for the fabrication of diffraction gratings because they are highly reflective and are chemically stable at ambient environments [43]. Moreover they are compatible with the electron-beam-lithography (EBL) fabrication technique (see 3.1.4). However gold is more preferred, because it is a noble metal that does not need a protective transparent layer [6].

2.4 Adhesion of Metallic Gratings to Polymers

The material system of interest in this thesis, consisting of the inorganic layer and the polymer substrate, dictates to address the process of bonding them together and to understand the physical mechanisms and the chemical features of the surface interactions involved. In the next paragraphs, the qualitative basic meaning of adhesion and the different experimental values of the adhesive junction are presented. The difficulties related to the measurement of the joint strength are discussed and two mechanical test methods for adhesion measurement are also provided as an example. The main advantages and limitations of each technique are discussed.

2.4.1 Fundamentals of Adhesion

Adhesion describes, in the simplest qualitative definition, the state of two similar or different materials sticking to each other by means of interfacial forces over the contact area [41]. The connecting forces are either of chemical nature, consisting of valence forces, or of mechanical nature, expressed by the interlocking forces, or both [12].

However, the quantification of the phenomenon is difficult, since it is impossible to measure the basic adhesion of the material system investigated [14]. In practice, the processes involved in the bond formation are dynamic and irreversible; while the existing adhesion theories work on the basis of static and reversible processes [45].
Thus, in terms of quantities, adhesion is considered in three different forms: the basic adhesion, the thermodynamic (or reversible) adhesion and the experimental (or practical) adhesion [14].

a. Basic adhesion:

The basic adhesion refers to the strength of the forces holding the two materials in contact together on a molecular scale. These forces could be either:

- Primary valence type (such as ionic, co-valent, metallic…)
- Pseudo primary valence type (i.e., hydrogen bonding)
- Secondary valence type (Van der Waals forces).

Neither the magnitude of this adhesion nor any of the adhesion forces can be calculated or measured in practical systems.

b. The thermodynamic or reversible adhesion:

The thermodynamic or reversible adhesion describes, as the name suggests, the reversible work required to build the interface between the assembled bodies [40]. It describes simply the energetic states of the system before and after the bond, which are quantified by surface energies (γ) and can be expressed as follows:

$$\mathcal{W}_{AB} = \gamma_A + \gamma_B - \gamma_{AB}$$

where $\mathcal{W}_{AB}$ is the reversible work of adhesion, γ_A the surface energy of body A, γ_B the surface energy of body B and γ_{AB} is the interfacial energy.
This thermodynamical approach is not helpful in case of thin film adhesion measurements, since the various parameters are not known and the work of adhesion cannot be determined. Nevertheless, it is normally used to calculate the work of adhesion between two liquids or between a liquid and a solid.

c. Experimental or practical adhesion:

The practical adhesion can be experimentally measured, either in terms of the forces applied to disrupt unit area of the interface, or in terms of the work done to separate two materials from one another.

The practical adhesion value can be defined as the sum of the basic adhesion strength plus the losses caused due to internal stresses and additional processes originating from the measuring procedure.
An accurate estimate of the joint strength is even in this adhesion manifestation not possible, since the added stresses and processes strongly vary from technique to technique and are sometimes even dependent on the operator's experience.
It is also imperative to mention that most of the test methods are originally established for bulk materials. The use of some of these techniques for the studies of polymeric and thin metallic film joints brings with it inevitable difficulties due to the viscoelastic nature of polymeric films [40].

2.4.2 Joining Metals to Polymers

The problem in binding metals with polymers originates from the large difference in their surface energies [65]. This discrepancy hinders a good bond formation and requires surface treatments to enable the adhesion. Binding metals to polymers involves several modifications, at the adhesive interface as well as the interphase layer. The bond formation at the interface is ensured by the functionalization of the polymer surface that leads to an acid-base reaction with the metallic oxide [14].
The surface treatments modify the interface surface by altering the physical structure, changing the surface topography, changing the chemical nature of the surface or removing a weak boundary layer. In this context, metals and low energy polymers mostly need surface treatment prior to bonding [14].
The metal surface is prepared for bonding, through the removal of surface contaminants, the existing oxide layer, and some of the underlying metal. This leads to the formation of a new oxide with better uniformity and strength [14]. The adhesion of thin films (usually < 1 µm and in some applications of the order of tens of nm) is influenced by the substrate features and properties including its type, its temperature and its surface condition. In addition, the adhesion is affected by the nature and thickness of the deposition material, and by the deposition parameters especially the deposition rate and pressure [40].

2.4.3 Adhesion Measurement Methods

2.4.3.1 Adhesion Main Theories

In polymer-metal bonding, the final joint strength depends on a number of factors [12]:

- chemical bonding,
- mechanical interlocking,
- electrostatic attraction between the metal and the polymer substrates,
- and the possible formation of weak boundary layers.

In addition, the close and intimate contact between the joined bodies is very important for a good adhesion. It is nevertheless to be considered, to avoid internal stresses in the materials or to achieve a plastic deformation of both of the entities upon pressure. Otherwise, the joint will be broken as soon as the external load is released [41].

2.4.3.1.1 Electrostatic/Electronic Theory

When a polymer and a metal are brought into very close contact, electrostatic forces between the two materials are generated, creating oppositely charged surfaces that attract each other. This electrostatic attraction is believed to be very modest compared to the strong intrinsic molecular forces of the basic adhesion [12].

2.4.3.1.2 Chemical Bonding

As mentioned above, the modifications of the contact surfaces of the metal or the polymer are essential to provide a strong and a durable joint.

Polymer surfaces can be acid-etched, plasma or corona arc treated to create reactive polar groups that promote chemical bonding with the inorganic material of the system to be assembled. Metal surfaces are oxidized and exposed to air so that moisture can be absorbed. This leads to the formation of hydroxyl groups that can easily react with the polar groups of the polymer, e.g.:

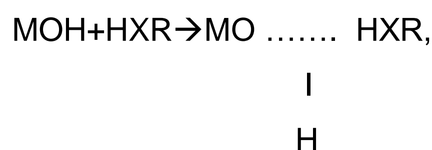

where M is the metal, H is hydrogen, X is an atom of oxygen, nitrogen or chlorine and R is a polar group [12].

2.4.3.1.3 Mechanical Interlocking

The modified surface topography may also promote a strong mechanical interlocking between the two bulk materials. The roughening of the contact surface of the substrate leads to the formation of more surface features favorable for the interaction with the adherent substance (Figure 20).

Figure 20: Micro-rough solid surface [14].

Such features like pores, depressions and asperities provide a larger contact area and promote therefore the mechanical interlocking of the materials [14].

2.4.3.1.4 Weak Boundary Layers

Bikerman postulated that, between two substances in contact, exists always a weak boundary layer [44], and that the destruction of the bond by the separation of the components is not an adhesive failure along the interface, but rather always a cohesive failure that takes place in this boundary layer.

The possible formation of such surface layers is explained by “the diffusion of lower molecular weight fractions to the outer polymer surface” [12]. Brockman “has suggested that 20 to 100 Å diameter polymer molecules can penetrate the interstices in the oxide film and lead to the formation of weak boundary layers” [12].

2.4.3.2 Mechanical Adhesion Tests

Adhesion of thin films can be measured through different ways, including mechanical testing. An ideal adhesion test, taking into consideration all the theoretical aspects, does not exist, and there are many limitations to the currently used methods [25].

For example, some of the currently used techniques do not provide absolute values to quantify adhesion, but are still useful when comparing relative changes. In addition, the results of different adhesion measurement methods cannot be directly compared to each other [40]. A common classification criterion for mechanical tests is

the way the force is applied to disrupt the interface between the two surfaces of the thin film and the substrate. This detachment can be applied perpendicular to the interface (e.g. Pull-off test) or in lateral direction (e.g. Peel test).

2.4.3.2.1 Pull-off Test

Procedure [40]

Pull-off studs, which are usually metallic cylinders, are glued to both the substrate and the thin film coating with cement (Figure 21). Then, a vertical pulling load is applied and the force is increased gradually until fracture occurs. Force vs. time measurement is taken during the test and the result is the average fracture stress.

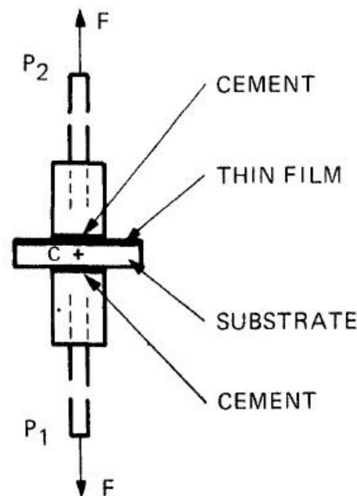

Figure 21 : Diagram of pull-off test. The force F is applied at cylinders P_1 and P_2 with the force aligned through the center C of the substrate [40].

Limits

- The test can be successful only if the fracture occurs at the coating-substrate interface and not at any other component such as the glue or the studs. This method is therefore limited by the strengths of available adhesives.
- A good alignment of the pull off-studs must be guaranteed; else angle deviations would lead to the peeling of the coating instead of the perpendicular pull-off.
- A risk of non-uniform stress distribution along the coating/substrate interface may lead to wrong interpretations. However, if most of the system components are not changed, the test can be used for ranking purposes.

2.4.3.2.2 Peel Test

Procedure [40]

The peeling of the coating from the substrate is ensured by applying lateral stresses to cause the detachment between both materials.

This can happen either by pulling directly on the film, or through some in-between materials called backings (Figure 22).

The most common peeling angle is 90° and there are many machine setups to ensure this constant angle over the test.

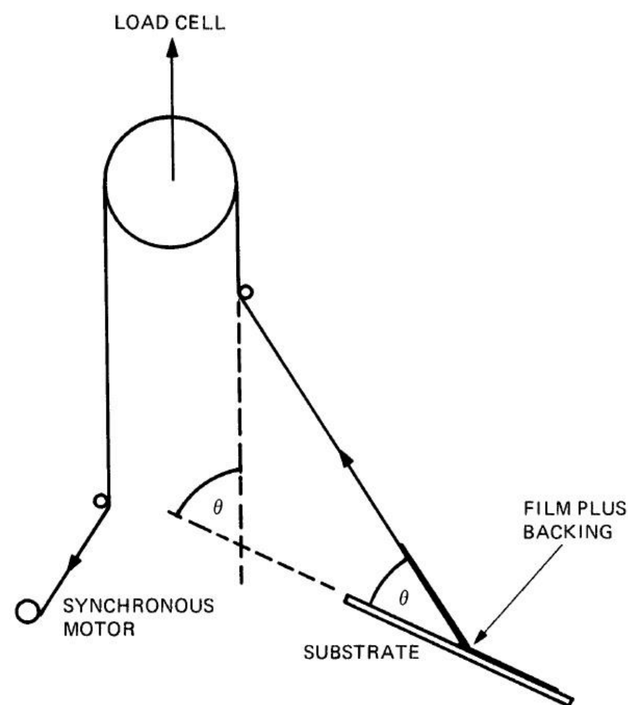

Figure 22: Schematic illustration of a peeling test apparatus [40].

Limits

Since it is not possible to determine the area of contact throughout the test course, the result of the test is not based on the measured force, but expressed as energy or work per unit area. It is therefore not directly comparable to the result of other force-based testing procedures.

In addition, having a good result at this test depends on the total removal of the film from the substrate. Therefore, it can be applied only to the interfaces with relatively poor adhesion.

3 Processing of Grating Couplers

3.1 Basic Fabrication Methods

The grating coupler configuration is very important in the field of nano-scale technology, particularly for the fabrication of sensors, since it allows a compact design and a good integration.

In order for the sensor to reach a good performance level, high quality and accuracy are needed to fabricate its small features [2].

The micro- and nanometer-scale patterns of the grating are commonly generated with the following techniques [59]:

- Scribing,
- Phase masks,
- Lithography including photolithography, electron-beam direct writing (EBL) and interference or holographic lithography (IL),
- Etching methods; mainly dry etching, such as reactive ion etching (RIE) and focused ion beam etching (FIB).

However, these different techniques are mostly used in a similar fabrication scheme: First, the shape of the structure is written on a photoresist by lithography and etched to form the patterns. Then, this etch mask is used to transfer the patterns to the underlying substrate [59].

The selection of a fabrication technique is dependent on the desired quality, geometrical period, total surface area of the structures and the materials that will be used. These basic techniques will be presented in the next sections and explained.

3.1.1 Mechanical Processing

This method is also known as scribing or ruling [39]. It is based on a mechanical process using a sharp instrument to cleave the surface of the substrate and form the pattern of the grating. Blazed gratings can be well fabricated with this method. It is mainly used to create master gratings for replication purposes. The smallest grating period realized with recent advanced ruling engines is 0.8 µm. However, it is to note that these engines are very costly and very slow [18].

3.1.2 Phase Masks

A phase mask is a precision diffraction grating that is optimized to split an incident light beam into two diffracted beams to record other gratings. Phase masks are mostly used in the +1/-1 or 0/-1 configuration, where the integers mean the diffraction orders of the diffracted beam. The interference pattern is created in the overlapping area [18] and recorded in the photoresist achieving periods ranging from a few hundreds of nm to 2 microns. Figure 23 shows the operation of a phase mask in the +1/-1 configuration.

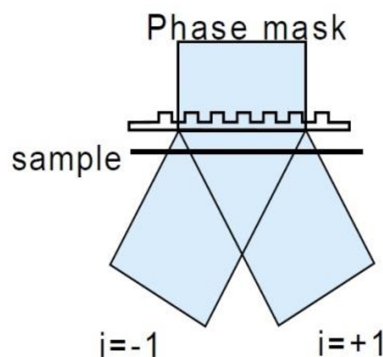

Figure 23: Operation of a phase mask [18].

Phase masks offer the possibility to be used in standard photolithography settings. But, the fabrication of the phase mask can be very expensive.

3.1.3 Photolithography

Photolithography uses ultraviolet (UV) light to transfer the patterns present on a predefined mask into a photoresist layer. The exposure induces changes in the chemical properties of the polymeric photoresist; and thus, the illuminated areas can be removed during the development. The patterned photoresist is then used as a mask to transfer the pattern to the underlying substrate by an etching technique. Figure 24 shows the process of creating a diffraction grating [18]. There are several variants of photolithography, and the choice of the appropriate method depends on the needed feature size. Contact lithography for example, can create slits down to 0.8 μm [58], while deep UV-lithography (DUV) can fabricate nano-scale patterns as small as 90 nm [2]. DUV is also a well established fabrication technique for mass production [59].

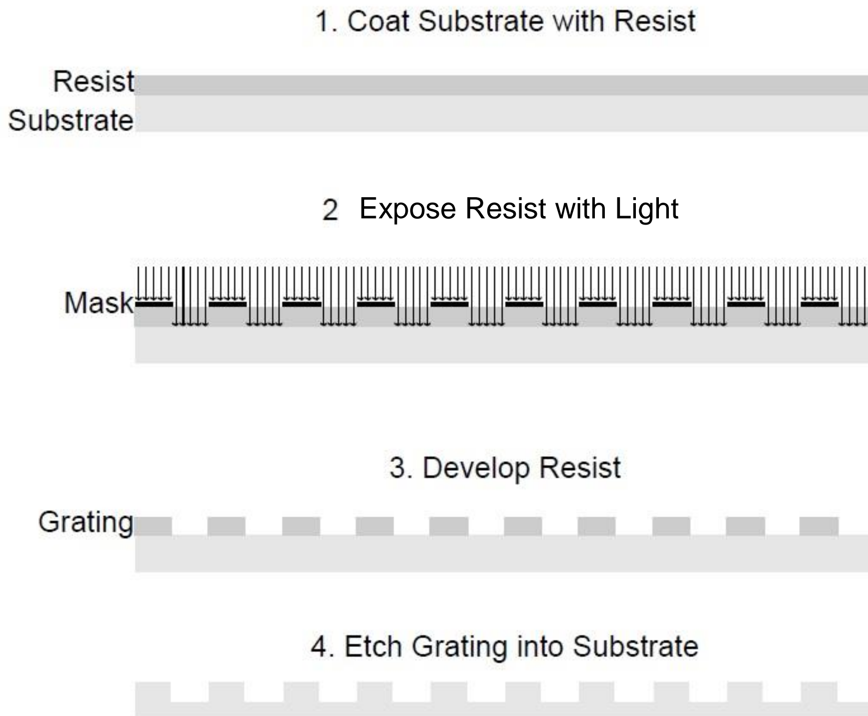

Figure 24: Contact photo-lithography process for grating fabrication [18].

3.1.4 Electron-Beam Direct Write Lithography

This EBL technique uses a focused electron beam to define the patterned structure directly on the resist without the use of a mask [59].

Adding to the flexibility of the system, the spot-size beam can be as small as 5 nm, providing therefore the possibility of fabricating small features of about 20 nm [2]. Yet the technique is not suitable for mass production and is usually limited to small areas since it is extremely time consuming [18].

3.1.5 Holographic Recording / Interference Lithography

Interference lithography is a fast and non-expensive nanofabrication technique used over the entire sample to record diffraction gratings with small periods. The period is simply determined by the angle between the two used interfering laser beams, as shown in Figure 25. The method can achieve grating periods down to about 240 nm [46, 59]. The total processed area depends on the beam size and could reach up to a few cm^2 [2].

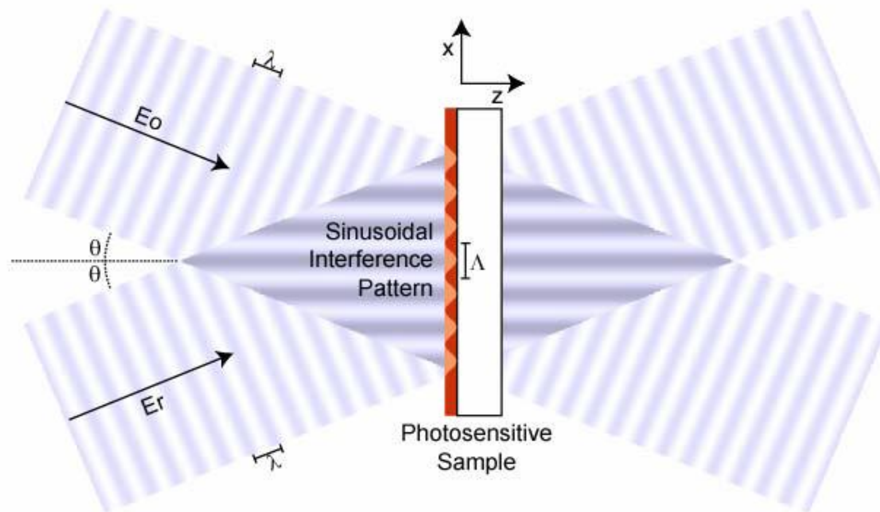

Figure 25: Holographic recording of sinusoidal diffraction grating [18].

3.1.6 Reactive Ion-Etching

Dry etching processes such as RIE [58] are used to effectively etch vertical walls. The process is conducted in a vacuum chamber filled with gases and is based on the generation of plasma to achieve the etching by the reactive ions. The nature of the used gases is an important factor in the choice of the materials that can be etched. By controlling the etch time, different etching depths can be achieved. The error on this depth can be under 5 nm, if the fabrication environment is well controlled [46, 59].

3.1.7 Focused Ion-Beam Etching

The FIB etching technique is similar to EBL, but uses a beam of heavy ions instead of electrons to etch a semiconductor or a metal directly. The method is a serial process with a low etch rate, which results in high accuracy in the features. Complex structures with variable geometries can also be realized with this good tunable technique [58]. But, it also brings with it the same drawbacks as EBL. For instance, the process can be very slow and limited to small areas of maximally a few hundreds of μm^2 [2].

3.2 Current Fabrication Schemes

3.2.1 Superplastic Nanoforming

In [52], a superplastic nanoforming fabrication process for reflective interference components, such as diffraction gratings, was presented. Metallic glass was used for the grating material because of its excellent nanoformability, mechanical and functional properties. The technique employs an interference optical system and generates nanopatterned microdies by large area circles of 5 mm diameter lithography, thus showing its big advantages for mass production compared with the EBL method. The diffraction grating was then fabricated with these dies by superplastic forming of Pt-based metallic glass.

A Pt-based metallic glass, having a T_g of 502 K (228 °C), was used with a working temperature of 540 K (266 °C), under a compressive load of 10 MPa and for a duration of 300 s. The process flow is described in the following section and depicted in Figure 26.

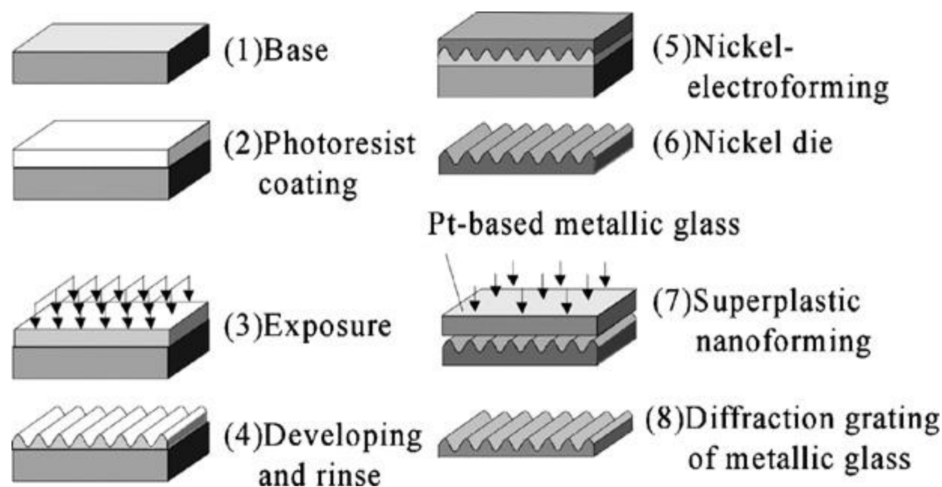

Figure 26: Fabrication process of a diffraction grating die by lithography and Ni-electroforming processes [52].

Fabrication steps:

The fabrication process of the diffraction gratings (as shown in Figure 26) is as follows:

(1) The Pt-based glass rigid substrate of choice is first prepared.

(2) A positive resist is then spin-coated on the substrate.

(3) The coated substrate is subsequently exposed to a solid-state laser of 375 nm wavelength by an interference optical system. The angle θ between the interfering waves (Figure 27) determines the period of the patterns.

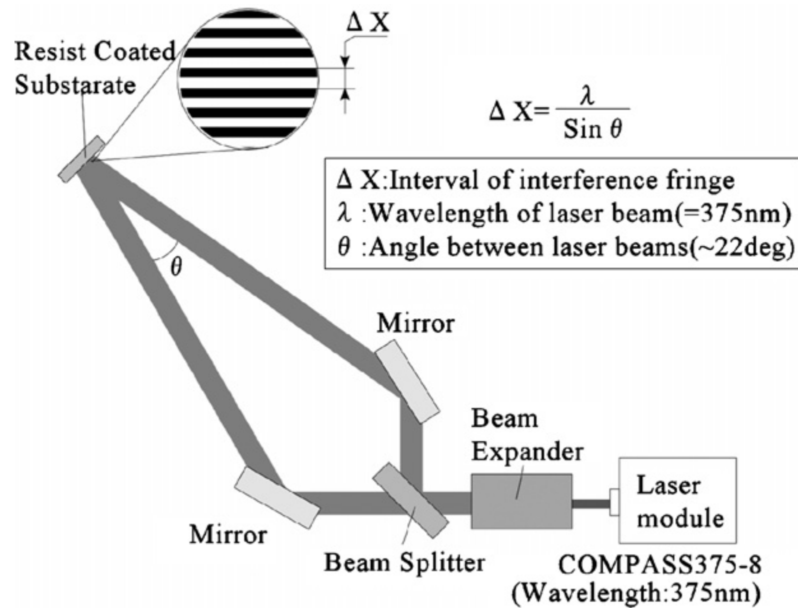

Figure 27: Configuration of one-shot exposure by an interference optical system [52].

(4) The sine-wave patterns of 1 μm interval are fabricated after development and rinsing; and the resist master for further processing is obtained.

(5) The micro shape of the resist is transferred to a Ni-micro die by electroforming in a sulfamate bath.

(6) The Ni-dies for the grating generation are formed.

(7) The diffraction grating is finally fabricated by nanoforming of the metallic glass using the resulting Ni-dies. The shape of the resist is transferred to the metallic glass with high precision, and the nanoforging is performed according to the following configuration:

- The metallic glass substrate and the Ni-die are placed between two separately heated plates, and a compressive load is applied. The plate temperatures and the pressure are controlled during the fabrication. The superplastic nanoforming machine is installed in a vacuum chamber to prevent the oxidation of the grating material and the penetration of air in the die.

- The superplastic nanoreplication of Pt-based metallic glass is performed under a compressive stress of 10 MPa, a forging temperature of 550 K (276 °C) and a working time of 300 s. The metal grating with the shape structure of the resist is obtained.

3.2.2 Flip Chip Double Side Processing with a BCB Adhesive Layer

This paper [19] presents a novel metal grating design for both, SOI and III-V based platforms. The buried SiO_2/Ag grating (Figure 28) was fabricated with well known standard processing methods and yet achieved a high efficiency independently from the benzocyclobutene (BCB) buffer thickness, and significantly decreased the parasitic leakage of light to the substrate.

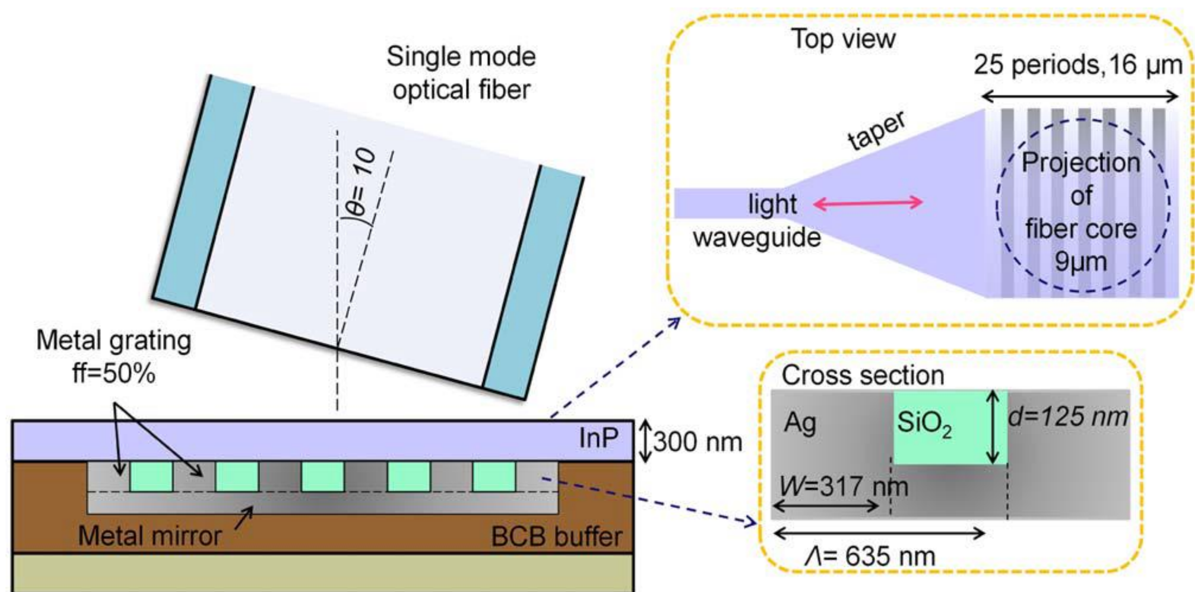

Figure 28: Schematic of the buried metal grating design [19].

The design parameters (Figure 28) calculated for a maximum theoretical efficiency of 74% are as follows:

- λ=1.55 μm wavelength of the input light,
- Coupling angle θ=10° and coupling distance away from the grating=10 μm,
- Grating period Λ=635 nm,
- Groove depth (of SiO_x) d=125 nm,
- Waveguide width=400 nm, waveguide thickness=250 nm.

Procedure and fabrication steps:

The metal grating is first defined on the III–V wafer. After adhesive bonding to a silicon wafer, the waveguides are etched in the thin Indium-Phosphide (InP) membrane.

The layer stack, as depicted in Figure 29, consists of an InP membrane of 300 nm thickness bonded to silicon by a 50 nm thick layer of SiO_x on top of a BCB layer of 600 to 900 nm thickness.

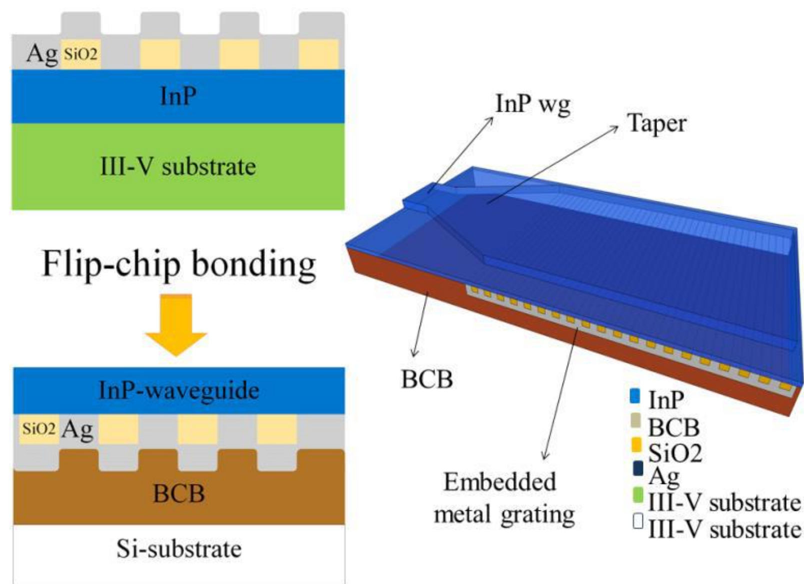

Figure 29: Schematic flow of metal-gratings fabrication and 3D view [19].

The fabrication steps can be summarized as follows:

1. At first, the alignment markers for the following overlay exposures are patterned through a 1st EBL. For that, a 320 nm thick positive resist was used on top of a 300 nm thick SiNx hard mask. The pattern is transferred from the resist to the SiNx by reactive ion etching (RIE) with fluorform (CHF_3). Then, the semiconductor layers were etched by inductively coupled plasma (ICP) to a depth of 690 nm with methane hydrogen (CH_4/H_2) at 60 °C. The SiNx mask is removed with Buffered Hydrofluoric Acid (BHF).
2. The fabrication of the grating:
    a. This begins with patterning stripes in SiOx (Figure 30). First, a layer of 125 nm thick SiOx is deposited using plasma enhanced chemical vapor deposition (PECVD). A 2nd EBL step is then performed with a positive

resist to define the stripe pattern with the design configurations, which is etched via RIE using pure CHF_3 chemistry. The residual resist is finally removed by oxygen plasma.

b. The oxide stripes are as next fully covered with silver (Figure 30). A 3rd EBL step for metal lift-off using an 800 nm thick PMMA resist to cover the SiOx gratings was first performed. After that, a 2 nm thin layer of germanium (Ge) followed by a 300 nm thick layer of silver are deposited in an electron beam evaporator under vacuum in a single-step method (conventionally the metal layer is thermally deposited). This novel approach improved the performance of the device through the better deposition uniformity, and by decreasing the optical losses in the metal layer. The Ge serves as a sticky adhesion layer for the Ag on top of the SiOx. The lift off is then performed submerging the sample to 1 h of acetone vapor followed by 1 h of liquid acetone and rinsed afterwards with acetone and propanol.

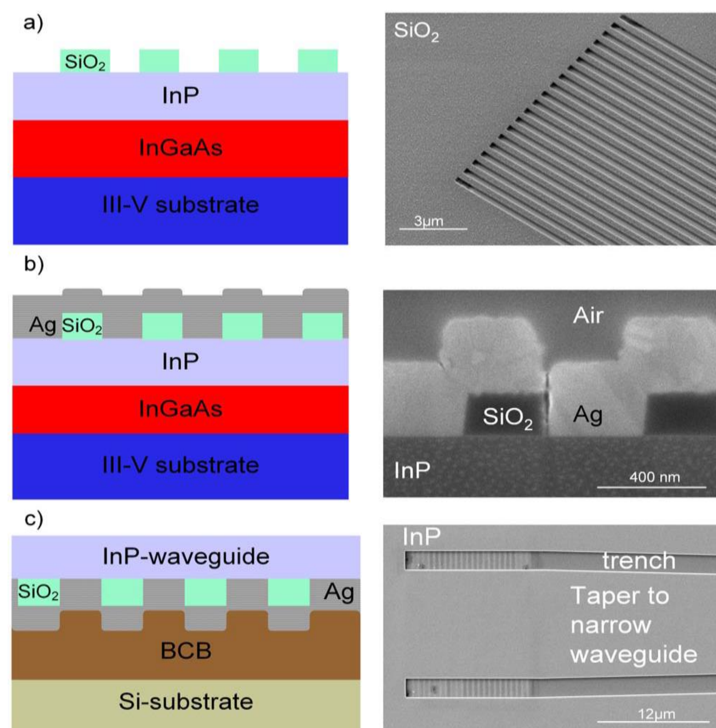

Figure 30: (a) Second EBL step: cross section of the SiOx pattern. (b) FIB cross section of the metal grating (with 175 nm thick SiOx) before bonding. (c) Fourth EBL step: cross section of the bonding and top view SEM picture of the fabricated metal gratings [19].

3. After silver deposition, the III-V chip is bonded to a silicon (Si) substrate using an adhesive BCB layer. Here, the Si wafer and III–V chip are prepared as follows:
   a. A 3 inch Si wafer is cleaned and 1000 nm of SiOx is deposited as an optical buffer layer between the InP membrane and the silicon substrate. Then, a BCB layer with a thickness of 900 nm is spun on the Si wafer and partially cured by heating the sample at 180 °C inside a vacuum oven for 1 h.
   b. Meanwhile, 100 nm of SiOx are deposited on the III–V chip to promote adhesion to the BCB.
   c. After curing, the III–V chip is placed epi-side down on the silicon wafer and is introduced into a bonding machine with a specific compressive force of 25 N/cm^2 and 280 °C for 1 h. The final thickness of the BCB that can be achieved with the machine is between 600 and 900 nm. Finally, the InP substrate of the III–V chip is removed with HCl/H_2O for 30 min at 35 °C.
4. At last, the patterning of the InP membrane with waveguides is conducted with a 4th EBL. For this, 2.5 µm long and 400 nm-1.5 µm wide trenches are patterned in a positive resist to define respectively the waveguides and the tapers. A 100 nm SiNx hard mask is deposited on the wafer, and followed by spinning of a resist. Nitride RIE and ICP steps are performed to transfer the pattern to a maximum of 250 nm depth into the InP membrane in order to avoid exposing the oxide or the BCB layer to the HF chemistry when removing the SiNx hard mask.

3.2.3 Nanoimprinting

A novel nanoparticles (NP)-film coupling system was proposed in [69]. The system consists of a double resonance substrate made of a conventional gold nano-particles array and an underlying silver grating film, suggested for the first time for such coupling substrates (Figure 31).

The novel system is based on a simple method, and achieved a very high enhancement factor thanks to the multiple couplings between the gold NPs and between the silver film and the gold NPs.

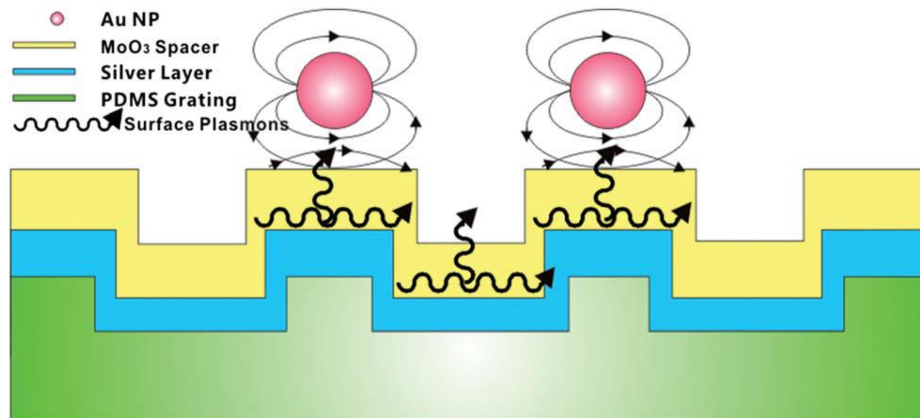

Figure 31: Schematic of the fabricated double resonance substrate [69].

Nanoparticle–film coupling systems consist basically of a layer of metal nanoparticles, a spacer and a flat metal film supported onto a substrate. Figure 31 gives a schematic representation of the fabricated sample with a silver (Ag) grating film.

The silver grating is characterized using a clear surface plasmon polariton (SPP) [69] effect in the system. The layer of gold NPs array shows a so called localized surface plasmon (LSP) [69]. This double plasmonic effect generated by the material combination results in a strong field enhancement near the surface of the nanostructure.

Fabrication of the double resonance substrate:

The fabricated device consists of:

- A gold nanoparticle array formed of gold spheres with a diameter of 25 nm and a period of 30 nm,
- A molybdenum trioxide (MoO_3) spacer with a thickness varying from 2 nm to 70 nm, with critical effect on the resulting field enhancement,
- And continuous 100 nm thick silver grating film.

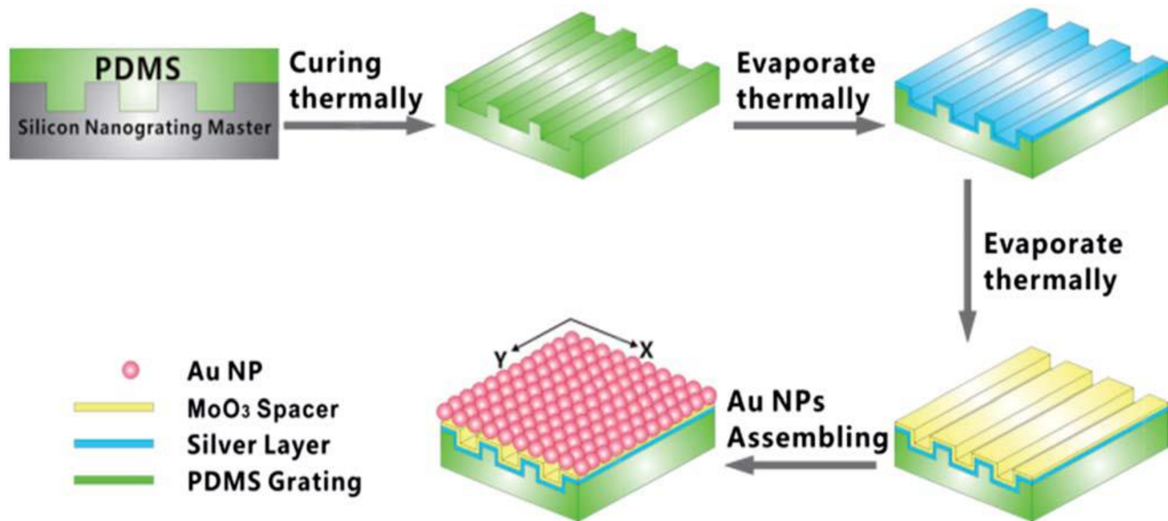

Figure 32: Schematic representation of the synthesis of Au NPs/MoO_3/Ag grating double resonance substrate [69].

The synthesis of the double resonance substrate is presented in Figure 32 and described as follows:

1. Fabrication of the silver grating by nanoimprinting:
    a. Polydimethylsiloxane (PDMS) is first prepared by mixing an oligomer and a curing agent, and then poured onto the silicon nanograting master.
    b. After removing the air bubbles and thermally curing at 79 °C for 3-4 h, PDMS molds were obtained with the dimensions of the master grating.
    c. An 80 nm Silver layer followed by a MoO_3 spacer with different thicknesses are then thermally evaporated onto the PDMS grating mold under vacuum at 10^{-6} Torr. The resulting grating has a period of 350 nm.
2. Fabrication of Au NPs: the synthesis of Au NPs was performed using the chemical reduction of chloroauric acid with sodium citrate method.
    a. A $HAuCl_4$ solution was mixed with water with defined proportions and concentrations, and heated to its boiling point.
    b. Upon boiling, trisodium citrate tetrahydrate was added quickly to induce particle formation during prolonged heating under reflux for 30 min. Au NPs with a diameter of 25 nm were obtained.

c. The synthesis of Au monolayer film followed the gold nanoparticle self-developed assembly approach:
   i. A solution of mPEG-SH in deionized water was first prepared.
   ii. An appropriate polymeric solution was added to a concentration of colloidal Au NPs.
   iii. The sample was maintained for about 8 h at room temperature with stirring.
   iv. Finally, the solution was assembled onto a substrate, and closely packed NPs could be obtained.

3.2.4 Hot Embossing

In [60], a replication technique for the fabrication of high efficient grating structures into polymer substrates was presented (Figure 33). The blazed metal master gratings are fabricated by electron beam lithography (EBL) by tuning the electron dose across the grating period. The asymmetric triangular profiles are then replicated into the PMMA polymer substrate by embossing; and exhibited high in- und output efficiencies.

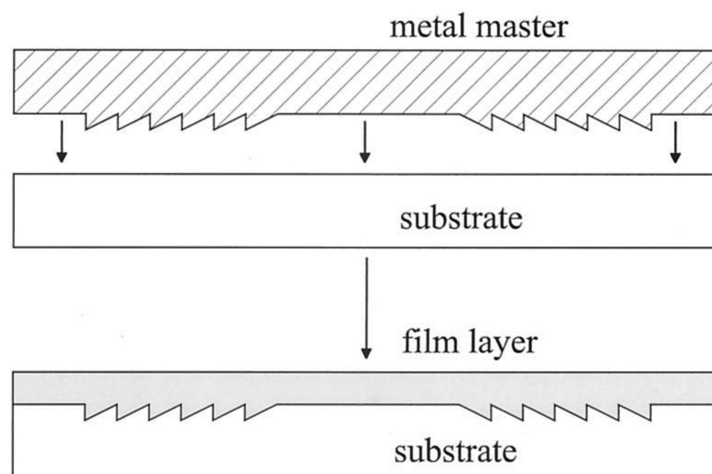

Figure 33: Embossing of the grating structure into the substrate [60].

Electron beam (EB) writing has several advantages, such as variation of the grating depth or the grating profile and realization of smooth, curved grating lines, which helps increase the coupling efficiency.

Fabrication technology:

- A thin film consisting of a copolymer of PMMA of less than 1 μm thickness is spin coated onto a quartz substrate. A thin metal layer of gold or aluminum on top of the resist is used to avoid charging during electron beam exposure.
- Linear gratings with straight lines and curved gratings with smooth curved patterns are written into the electron resist with two different electron-beam devices and by means of electron dose control.
- The fabricated grating with a period of 800 nm, groove depth of 250 nm, over an area of 1x1 m^2 and a thickness of 800 nm were replicated into nickel (Ni) by electroplating, resulting in 300 μm thick Ni master gratings.
- The metal master is then used for repeated embossing of the grating structures into 2 mm thick PMMA polymer substrates. The embossing procedure is as follows:
  - The PMMA plates are heated to a temperature of 150 °C.
  - Then, the grating structures are molded under the application of heat and pressure into the polymer by the metal master.
  - After cooling down, the wave guiding layer consisting of poly-methylstyrene (450 nm thick) was spin coated on top of the embossed grating structure. And the strip waveguides were fabricated by the direct-writing technique and developed to give the waveguide structure.

The fabricated grating was not coated with a metal.

3.2.5 Wet Etching

A polymer based surface grating coupler was presented in [62]. The device is fabricated with a simple and fast UV-based soft imprint technique utilizing self developed low-loss polymer material. The coupling efficiency is enhanced by embedding a thin Si_3N_4 layer between the polymeric waveguide core and under cladding layer (Figure 34). In addition to the enhanced efficiency, the technique can reduce the chip cost and achieve high volume production.

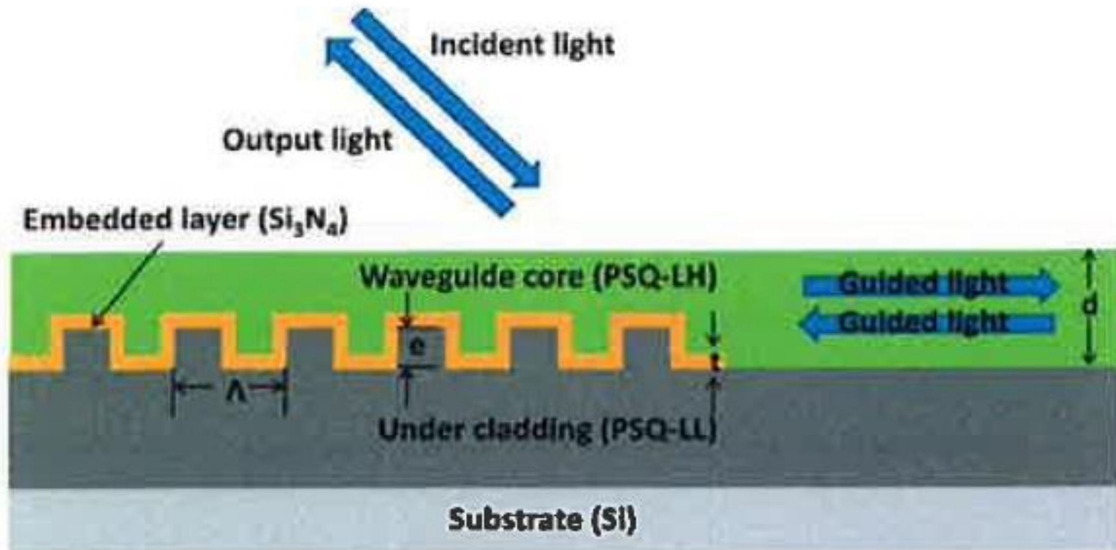

Figure 34: The proposed polymer-based surface grating coupler [62].

Design and procedures:

The used parameters were optimized for higher coupling efficiency and are as follows:

- Thickness of waveguide core d=1.7 μm,
- Grating height e=0.7 μm,
- Thickness of Si_3N_4 layer t=0.2 μm,
- Grating period Λ=1.7 μm.

Compared to lithography and dry etching, the developed technique in this paper has been proven to be an efficient way to directly pattern the polymer waveguide and devices. However, certain requirements on the imprinted material are needed:

- Good optical properties (such as low optical loss, low birefringence and high thermal stability).
- Good UV curing.
- Low viscosity.

The material used here is a kind of liquid polysilisiquioxane (PSQ) resin, with two components PSQ-LH used as the waveguide core with high refractive index (n=1.52) and PSQ-LL used as the cladding with low refractive index (n=1.45).

The fabrication process is shown in Figure 35 and described as follows:

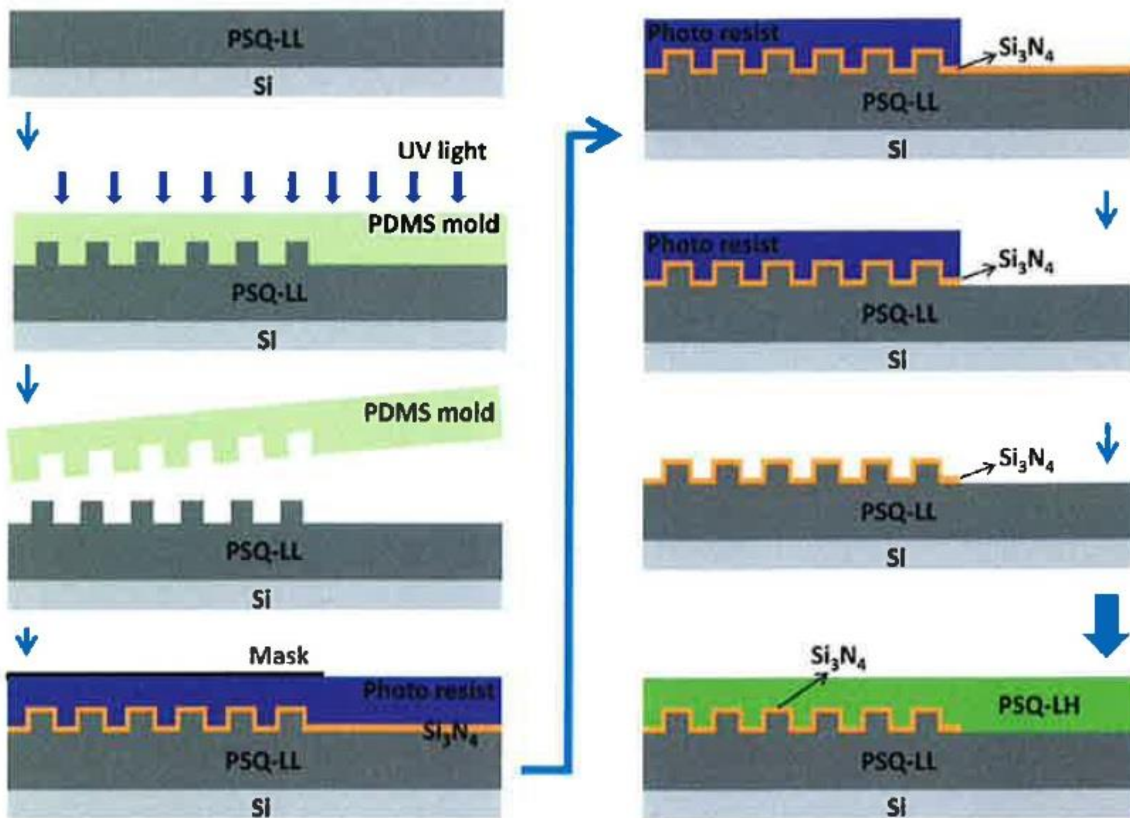

Figure 35: The fabricating process of UV soft imprint lithography combined with wet etching to realize the proposed structure [62].

1. The patterned PDMS soft mold is first fabricated by replication from a master mold on which the grating and waveguide patterns are defined by contact lithography.
2. The obtained mold is then pressed against the under cladding layer, which is spin-coated on the Si wafer, and then cured for 3 min with UV light.
3. The soft mold is peeled from the substrate leaving its patterns on the cladding layer. This layer is fully cured in 2 h at 180 °C.
4. Then, the selective Si_3N_4 embedded structure is realized:
   - The sample is coated with a 200 nm thick Si_3N_4 through a carefully optimized PECVD step. By experimenting, the deposition temperature was chosen to be 150 °C for a deposition time of 17 min.

- Rather than dry etching, a simple wet etching method with hydrofluoric acid (HF) solution was used to completely remove the Si_3N_4 layer from the waveguide region, leaving only the grating area covered.

5. After the spin coating and curing of the core layer PSQ-LH, the grating structure was realized. Figure 36 shows an SEM picture of the fabricated grating.

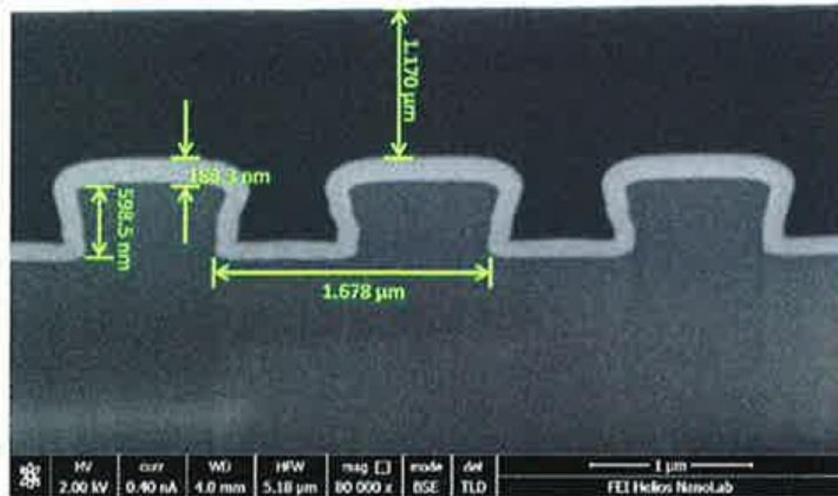

Figure 36: SEM picture of the fabricated surface grating coupler with Si_3N_4 layer embedded between the core and under cladding layer [62].

3.2.6 Mechanical Removal with Carbon Tubes

In [8], a novel mirco-machining process for the fabrication of sub-10 nm metallic gratings was presented. Carbon nanotubes (CNTs) were used as cutting tool to cleave corrugations in the metal coating and fabricate the grating structure. The success of this concept has been studied and demonstrated with a full scale molecular dynamics (MD) simulation.

The CNT has unique mechanical properties (such as high tensile strength, low thermal expansion coefficient, high thermal conductivity, high flexibility and elasticity) that could make it a good material for the cutting tool in micro scale manufacturing.

Procedures:

The machining process:

1. Starts with placing CNTs with equal and tunable distance on the rigid substrate,

2. Followed by coating a desired metal between and on the top of the CNTs (Figure 37),
3. Pulling the ends on the same side of CNTs (colored in orange in Figure 37) in the z direction with a constant velocity, results in the material removal by the CNTs and the grating pattern formation.

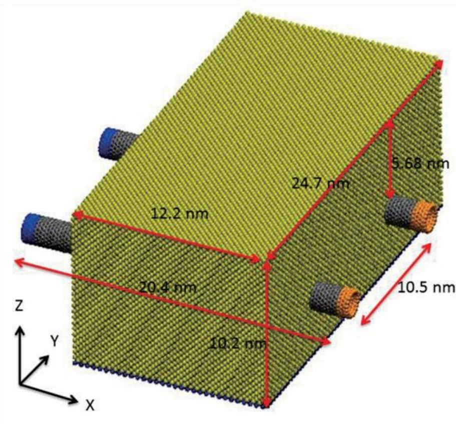

Figure 37: The physical model of the simulation with the metallic film structure and two open ended zigzag type CNTs [8].

The simulation is implemented under a canonical ensemble system with constant total number of atoms, constant system temperature (calculated to be 300 K) and constant system volume for the whole process. Figure 38 shows the material removal behavior by the CNTs, where the atoms are either individually disturbed in space, discharged into clusters or adherent to the CNTs.

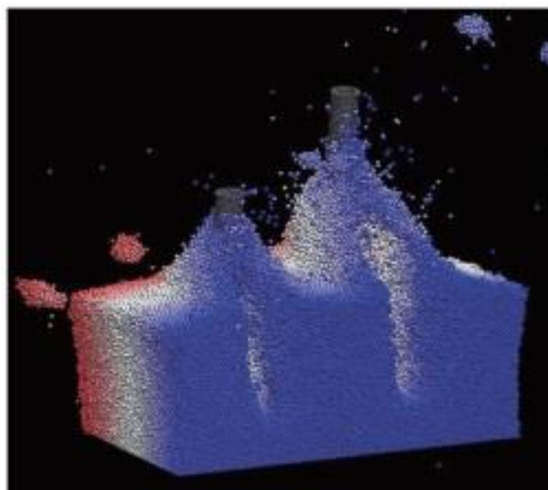

Figure 38: Snap shot from the simulation of the grating generating process [8], (No information was given about the color-scale).

Figure 39 shows the final form of the generated grating. Bending phenomena are obvious at the extreme sides of the gratings, while the center structure is almost unaffected. The same results were also predicted for large area and multi-CNTs processing. The material removal rate affecting these configurations is mainly defined by the steering velocity of the cutting tool. The study showed that small machining forces achieve better grating forms.

Post processing procedures can be adopted to remove the deformations, such as reactive ion etching.

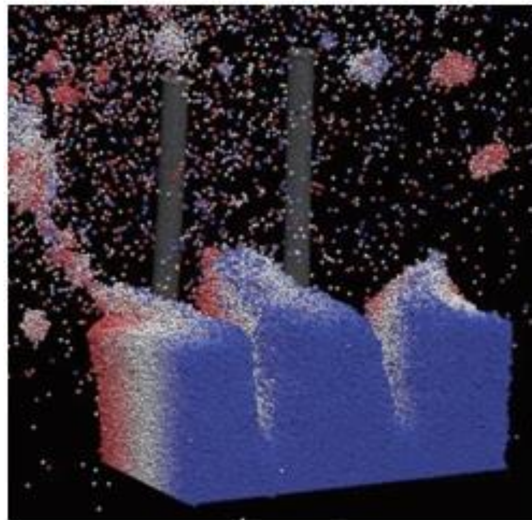

Figure 39: Snap shot from the simulation of the grating formation [8], (No information was given about the color-scale).

3.2.7 Stretchable Metallic Gratings

Yin. D. et al. presented in [68] a simple and flexible method for the fabrication of a submicron scale stretchable metallic grating with tunable periodic wrinkles on an elastomeric substrate.

Fabrication details:

The stretchable gratings (Figure 40) are fabricated as follows:

1. Transparent PDMS substrates are prepared by casting a mixed and degassed PDMS pre-polymer on the polished surface of a silicon wafer. Curing at 95 °C for 1 h produced PDMS sheets with thicknesses of 400–700 µm. The treated surface of the silicon wafer generates PDMS sheets and later gratings with a smooth surface.

2. After peeling off the PDMS sheet from the silicon wafer, rectangular substrates with desired sizes are cut.
3. The soft PDMS strip is then pre-stretched with 35% strain and treated with oxygen plasma to create a stiff skin on the substrate surface (step 1).
4. After releasing the pre-strain, wrinkles with desired periods are generated on the surface of the PDMS strip (step 2). The polymer wrinkles are used as next as templates for the fabrication of the metallic gratings. The template realized has a starting period of 560 nm and starting amplitude of 150 nm.
5. In step 3, the PDMS template was re-stretched with 30% strain and a thin silver film with a thickness of 25 nm was deposited. The second strain was applied to improve the mechanical robustness and morphology stability of the final metallic gratings. The second strain should also be less than the pre-strain, so that the wrinkles do not disappear by re-stretching.
6. Releasing the second strain finally forms the metallic grating wrinkles as shown in Figure 40 (step 4).

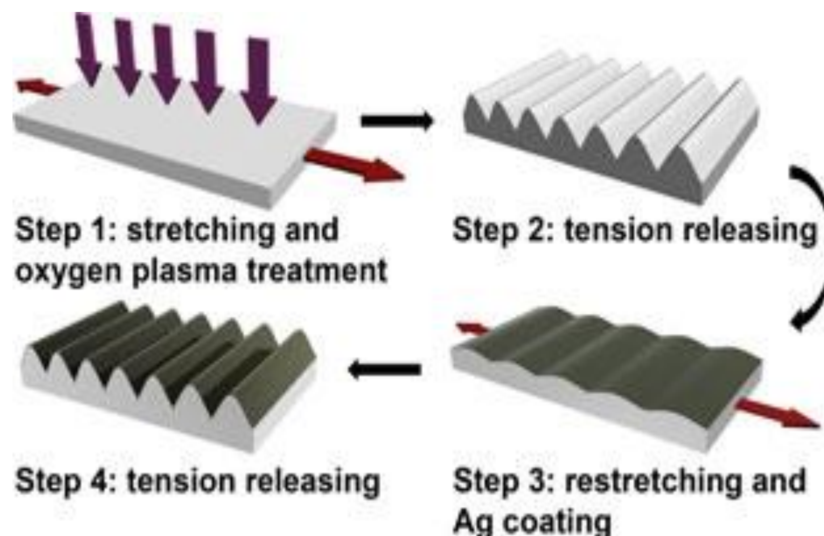

Figure 40: Schematic illustration of the procedure used to fabricate stretchable metal gratings.

The period of the templates and of the gratings can be controlled by tuning the duration of plasma treatment and by tuning the external mechanical strain, respectively. Periods ranging from 470-670 nm have been achieved.

3.2.8 Laser & Dry Etching

A novel approach to fabricate high quality sub-micron gold (Au) gratings with pulsed laser interference lithography (LIL) was presented in [2]. The method combines the use of laser interference patterning on a photoresist layer with conventional ion etching technique to achieve gratings with high resolution over large areas.

The limitation of the direct laser ablation (without the photoresist layer) lays in the fact that the high thermal energy of the laser pulse may deteriorate small periodic patterns as it melts the metal material.

Procedures:

The presented approach consists in:

- First recording the grating structures in a photoresist by means of the LIL,
- Then transferring the patterns to the metallic layer.

The fabrication process is based on the following steps schematized in Figure 41:

1. First, a Au thin film is deposited on borosilicate glass substrates:
    - The substrates were first rinsed by acetone and then cleaned with successive acetone and isopropyl alcohol.
    - After the cleaning process, a Au film with a thickness of about 60-80 nm is sputtered onto the sample with no adhesion layer between the gold and the glass substrate.
2. Then, a UV-sensitive negative was spin-coated in order to obtain a 300 nm thick photoresist layer. A pre-exposure bake was performed at 100 °C for 1 minute to remove the solvent.
3. Then, the LIL technique was used for the photoresist exposure with a frequency tripled nanosecond laser.
    - After irradiation, a post-exposure bake was performed at 110 °C for 1 minute and the sample was developed for 35 seconds at 21 °C. Immersing the sample in isopropyl alcohol for 60 seconds stopped the development process.
    - The sample was subsequently immersed in de-ionized water for 60 seconds and finally dried with nitrogen. Gratings with a very high level of uniformity and periodicity were then obtained.

4. The next step was to transfer the pattern from the photoresist to the underlying Au thin film using a dry etching process with argon (Ar) ions with optimized process parameters.
5. Finally, the remaining resist was removed by an ultrasonic Nmetil-2-pirrolidone (NMP) bath at 50 °C for 5 minutes, followed by two subsequent 5 minute rinsing steps with isopropyl alcohol at 50 °C and with distilled water at 50 °C. Gratings with a period of 770 nm and slit depths of about 55-60 nm were obtained.

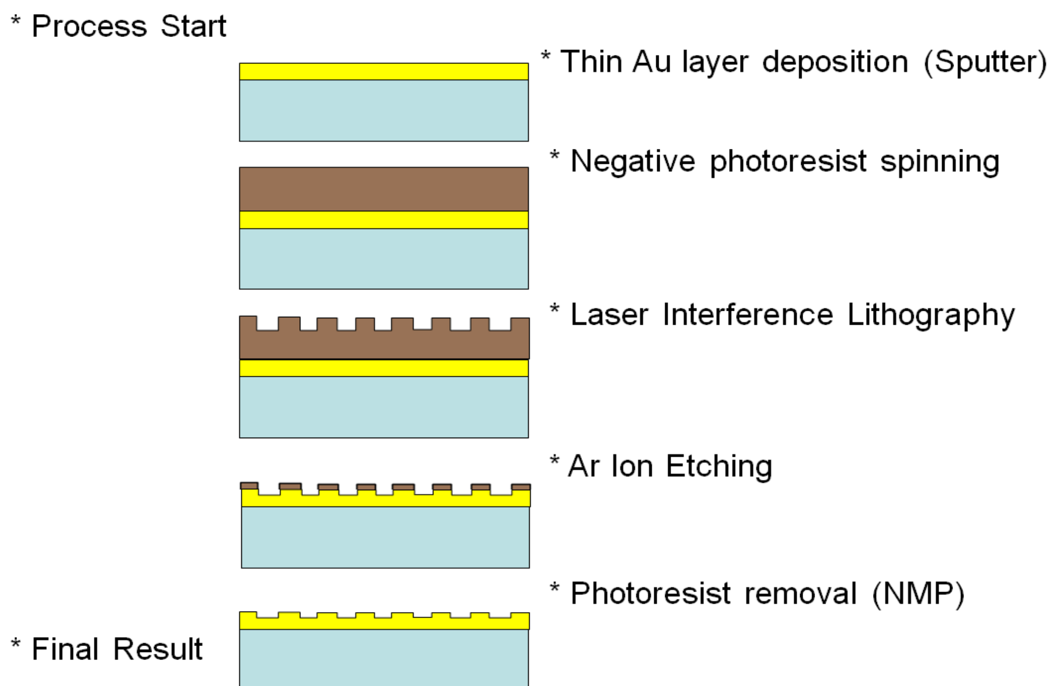

Figure 41: Schematic overview of the fabrication process [2].

3.2.9 Additive Nanopatterning

In [33], a simple and versatile contact printing technique was introduced. It leads to a nanometer resolution over large areas and can be conducted under ambient conditions. Noble metals as well as surface oxide forming metals can effectively be transferred based on various substrate/stamp combinations (rigid, soft).
The pattern transfer is ensured through the intimate physical contact between the stamp and the substrate without external pressure. A chemical reaction takes place between the metal patterns of the stamp and the targeted substrate surface. Both

materials form surface oxides, which leads to a subsequent hydroxyl group formation and ensures the chemical bond.

The method is purely additive and the stamps can be reused with occasional cleaning, thus reducing the cost of this nanofabrication technique.

Fabrication process:

The procedures of the patterning method are illustrated in Figure 42 and can be described as follows:

(a) The process starts with the stamp preparation. The geometry of the pattern is defined by the relief of the fabricated stamp.
   - Elastomeric stamps were prepared by casting and curing a prepolymer of PDMS against a pattern of photoresist on a silicon wafer.
   - Rigid stamps were fabricated by patterning a resist onto GaAs or glass substrates, followed by a RI-etching step of the exposed regions and finally by the removal of the remaining resist with acetone.

(b) Uniform layers of gold (20 nm) and titanium (5 nm) are then evaporated on the stamp. No primer is used on the stamp so that the Au does not adhere to it and can later be easily peeled off from the stamp.

(c) The stamp and the substrate are subsequently plasma oxidized in order to form hydroxyl groups on the surfaces necessary for the condensation reaction. PDMS thin films of 10-50 μm thickness supported on a PET polymer (175 mm thick) were used as substrates.

(d) The hydroxylated surfaces are then brought into intimate physical contact without external pressure to let the condensation happen at the interface. This chemical reaction results in permanent chemical joints between the metal film and the substrate.

(e) The complete transfer of the metal patterns (Au/Ti and Al) is finally performed under ambient conditions by separating the substrate and the stamp from each other after a contact time of less than 15 s.

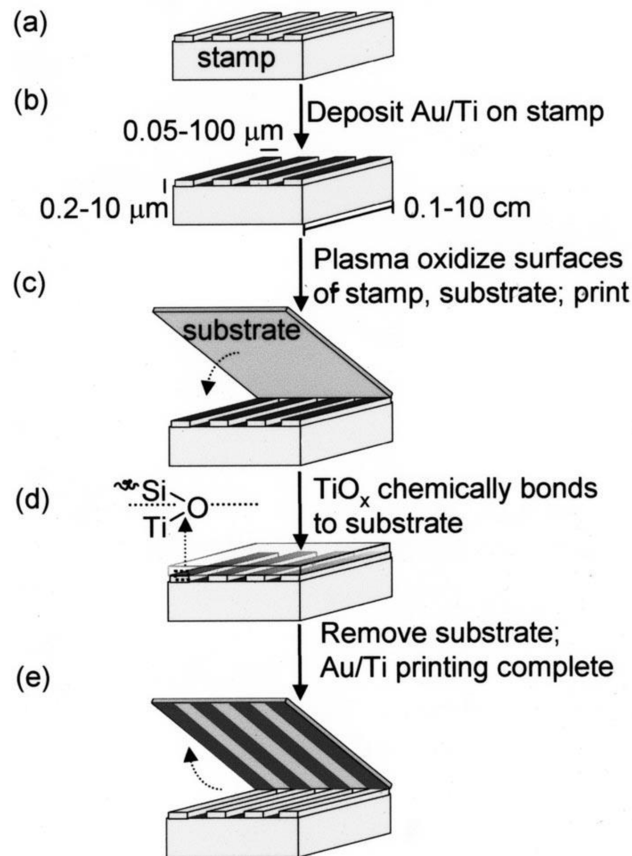

Figure 42: Schematic of procedures for nanotransfer printing (nTP) [33].

The metal coatings were completely transferred to the receiver substrate. The thickness of the Au/Ti layers is 25 nm.

3.2.10 Melt and Mold Fabrication

In [31], a simple, low cost and versatile replica molding technique for the fabrication of metallic gratings with small features (417-556 nm) was demonstrated.

The technique duplicates the geometry of a master device with a PDMS mold using low melting point metals and simple energy sources. The performance of the resulting replica depends mainly on the surface properties of the molten metal and can be improved by surface treatments and vacuum techniques.

The approach presented in this work used low melting field's metal and pure metal alloys and the melting process was conducted with either a Bunsen burner or a laboratory heating gun. Original aluminum gratings were purchased and used as received for the replication.

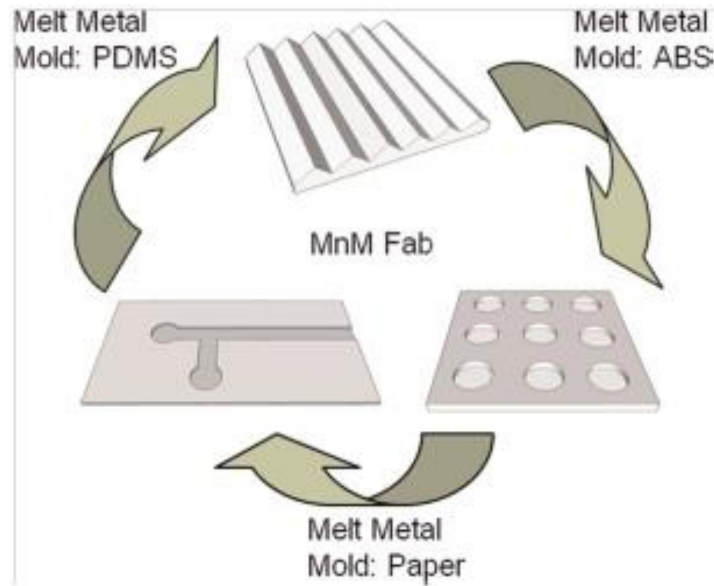

Figure 43: The melt & mold fabrication of various devices (diffraction grating, well-plates and micro fluidic devices) using the same metal and different molds [31].

The Melt & Mold duplication method:

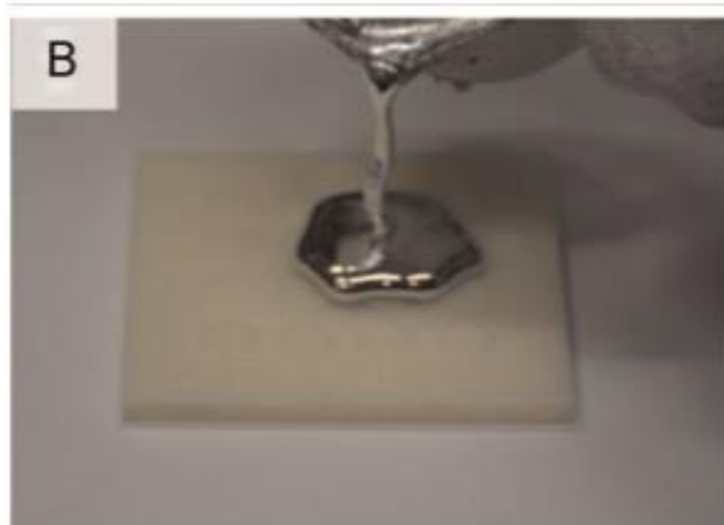

Figure 44: Molten metal being poured onto mold (example fabrication of a well-plate) [31].

The replication technique relies on the following steps:

- At first, the master mold is fabricated by covering the original grating in liquid PDMS and then cured for 2 h at 70 °C. The PDMS elastomer was prepared by mixing a prepolymer and a curing agent.
- The grating is then released from the PDMS mold, leaving its negative pattern in the soft polymeric mold.

- The diffraction grating replicas are then generated by pouring the molten metal (gallium, indium, Field's metal, and bismuth-tin) over the PDMS master mold (example in Figure 44) and then pulled off after cooling at ambient conditions (410 min).

3.2.11 Flip and Fuse

The novel technique presented in this work [1] consists in the coating of metallic materials on polymer substrates with low transition temperatures. The fabrication method is performed at ambient conditions and the diffusive mechanism between the two substrate materials is achieved by means of a thermo-compressive energy and an implemented adhesion promoter on top of the metallic layer stack.
Aluminum patterns of feature sizes ranging between 15-200 µm (1 µm thickness) onto polycarbonate film have been successfully fabricated with good design conformity.

Procedures:

The fabrication process is conducted as follows:

1. Starting with the preparation of the donor stamp in a 100 class clean room at 20°C and 50% humidity (Figure 45):

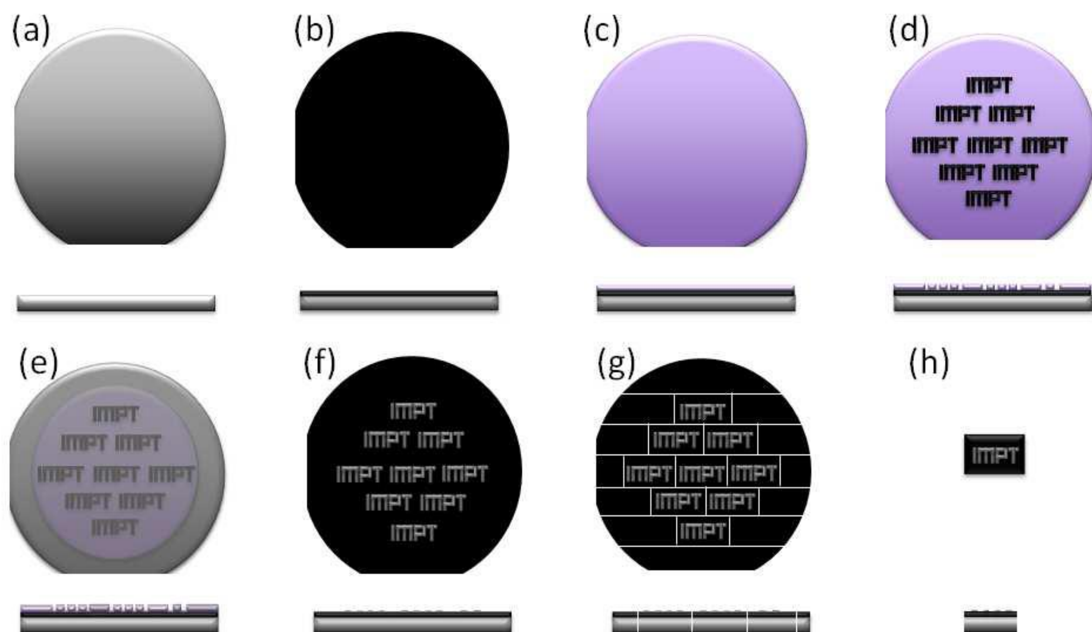

Figure 45: Donor fabrication process.

(a) A double side polished silicon substrate is cleaned and prepared.
(b) A thermosetting polyimide is then spin-coated on top of the silicon wafer and baked on a hot plate at 100 °C for 10 min. After cooling down to room temperature, the UV-exposed polyimide is fully cured at 350 °C for 1 h. The polyimide serves as a non-stick layer between the silicon and the metallic coating.
(c) A sensitive photoresist is then used for patterned coatings. The resist is cured before and after the UV-exposure, at 100 °C for 7 min and 110 °C for 1 min, respectively.
(e) After the development and rinsing of the resist, the metal of choice is thermally evaporated onto the stamp at room temperature.
(f) A lift-off is subsequently performed and the obtained stamp (g) is diced into single donor systems (h).

2. After the stamp preparation, the Flip & Fuse process is performed with the use of a conventional flip chip bonding tool. For this, both the coated stamp and the receiver substrate were heated, to 200 °C and 145 °C respectively and their temperatures were maintained constant during the entire process step. A subsequent compressive load of 2.5 MPa was then applied on the substrate/stamp system for 5 min until full saturation of the adhesive bond. The adhesion promoter used in this technique was an Indium layer of 50 nm thickness.
3. The rigid stamp was finally separated from the polymer film by centric bending and resulted in the pattern transfer. This approach ensures the ability of Flip & Fuse to be implemented in a roll-to-roll manufacturing process.

3.3 Overview Matrix

The researched processes are summarized in the next table, with emphasis on the used materials, the most relevant processing parameters, roll-to-roll compatibility and possibility of local processing.

Process Name	Grating / Substrate Material	Adhesion Promoter	Used Chemical & Physical Treatments	Processing Temperature	R2R Compatibility	Local Processing
Super plastic nano forming	**Grating:** Pt-based metallic glass T_g=502 K = 228 °C **Substrate:** Substrateless.	Nothing.	A solid-state laser (375 nm wavelength) used for resist patterning. Ni-electroforming for pattern transfer to master dies in sulfamate bath.	Working temperature T=540 K=267 °C.	-The one-shot exposure method has great advantages in manufacturing time and area compared with the EBL method.	The process generates metallic micro dies that can be individually placed on a substrate material; microstructures of an area of 5 mm diameter circle were fabricated.
Flip Chip with BCB layer	**Grating:** Silver (Ag) 125 nm thick. **Substrate:** SOI and InP membranes.	- Benzocyclo-butene (BCB) layer of 600 to 900 nm thickness to bond to silicon. - 2 nm thin germanium (Ge) sticky layer for the Ag on top of the SiOx.	- 1st EBL: RIE then dry etching on the inductive coupled plasma (ICP) machine and BHF chemistry. - 2nd EBL: PECVD of SiOx then RIE and oxygen plasma for resist removal and BHF for mask removal. - 3rd EBL: metal lift off in acetone vapor and liquid for 2h then rinsing with acetone and propanol. - 4th EBL: Waveguide patterning; ICP etching in SiNx and InP. Wet etching of the SiNx mask by BHF and HF.	- PECVD generally between 25-180 °C. - Electron beam-induced deposition (EBID) generally between 25-360 °C. No precise temperatures were mentioned in the reference.	- Conventional fabrication procedures but very time consuming EBL techniques and many process steps. - For the use on polymer substrates the process has to be adapted to satisfy material compatibility. -R2R compatibility: the method is complex since it contains many steps, but all the processing techniques may be adapted in a r2r operation.	Localized processing is possible but very elaborate and slow.

Process Name	Grating / Substrate Material	Adhesion Promoter	Used Chemical & Physical Treatments	Processing Temperature	R2R Compatibility	Local Processing
Nano imprint (gold nano particles)	**Grating:** Gold (Au) NPs (diameter of 25 nm) separated by a MoO_3 nano-spacer (thickness from 2 nm to 70 nm) from a Silver (Ag) grating film 80 nm thick. **Substrate:** PDMS.	No adhesion promoter.	Thermal evaporation of Ag under vacuum 10^{-6} Torr. Au NPs: chemical reduction chloroauric acid with sodium citrate, boiling and stirring at room temperature for 8 h.	T_{curing} of liquid PDMS =79 °C for 3-4 h.	-The distribution of the NPs has to be uniform and compact. - R2R compatible with vacuum requirement for metal deposition.	A heterogeneous integration on polymer films is needed after fabrication of individual gratings.
Hot embossing	**Grating:** No metallic coating used. **Substrate:** PMMA plates (2 mm thickness).	No adhesion promoter used.	No treatments used.	$T_{heating}$ = 150 °C of PMMA under Pressure.	-The technique is simple, fast and non-expansive due to reusable masters. -For R2R compatibility, the technique may be adapted for large area fabrication, as is the intent of the PlanOS project.	Grating areas of 1x1 mm^2 can be realized. Localized processing is possible since the master stamp can be freely positioned above the molding area, by a movable carrier for the embossing unit, for example.
Wet etching PSQ substrate	**Grating:** a 200 nm thick Si_3N_4 layer. **Substrate:** Liquid polysilisiquioxane (PSQ) resin. Two components: PSQ-LH with n=1.52 and PSQ-LL with n= 1.45 on silicon.	No adhesion layer used.	-Thermal curing of PSQ-LL in 2 h at 180 °C -Wet etching with HF to remove the excess of Si_3N_4 layer. -PECVD for metal coating at 150 °C.	Experimentally chosen deposition temperature of 150 °C.	-Simple, fast and non-expensive process yet needs vacuum for the metal deposition. -Wet etching has to be customized for the use on polymers. -R2R compatibility: fabrication steps may be accomplished using r2r processing.	Well established fabrication methods, but deliver single system that need to be additionally transplanted over large area flexible substrates.

Process Name	Grating / Substrate Material	Adhesion Promoter	Used Chemical & Physical Treatments	Processing Temperature	R2R Compatibility	Local Processing
Removal with carbon nanotubes (CNTs)	**Grating:** Gold has been used in the reference trial. No other materials are mentioned. **Substrate:** a rigid substrate.	Not mentioned.	No chemicals.	300 K (26,85 °C) thermal bath (canonical simulation system)	- A winder/ cylinder may be used to replace the steering velocity and cut the metal when bending the polymer film. - Time consuming: each CNT has to be placed at the right position. - Handling of several thousands of slits is hard and time consuming. - Costly: CNT are very expensive.	Through a master pattern, the supporting substrate can be selectively coated with the metal. The CNTs can be arranged separately on a moving apparatus and placed exactly where wanted for the metal deposition step.
Stretchable gratings	**Grating:** Silver (Ag) 25 nm thick. **Substrate:** Polydimethylsiloxane (PDMS) on polished silicon wafer (400-700 µm thick sheets).	Nothing.	Oxygen plasma treatment ranging from 2 to 5 min to form a stiff film on top of the soft substrate.	PDMS substrate was cured at 95 °C for 1 h. Plasma treatment generally between 15 and 90 °C for 2 to 10 min (no specific information were given in the work).	- R2R feasible by stretching entire sections of the polymer film and thus realization of large grating plates that can be cut in separate processing steps in smaller sizes to achieve wanted dimensions. - Procedure is not time consuming. - Two process modules are needed only: stretching stage and metal coating evaporator.	Localization not directly possible. 5 cm x 1 cm sheets can be created. Gratings may be fabricated on a large film and diced to produce single grating systems, then placed on a new substrate of choice.

Process Name	Grating / Substrate Material	Adhesion Promoter	Used Chemical & Physical Treatments	Processing Temperature	R2R Compatibility	Local Processing
LIL combined with dry etching	**Grating:** Au 60-80 nm. **Substrate:** Borosilicate glass substrates.	No adhesion layer.	Frequency tripled nanosecond pulsed laser energy (355 nm). Gold sputtered by Radio Frequency (RF) magnetron. For the substrate cleaning: acetone and isopropyl alcohol. AZ® 726 MIF developer for the cured sample at 21 °C. Isopropyl alcohol to stop the development and nitrogen for drying. To transfer the pattern to Au, Argon ion etching at 10 mTorr, NMP bath and isopropyl alcohol at 50 °C for resist removal.	Pre-LIL-exposure bake of the photoresist at 100 °C for 1 minute to remove the solvent. A post-exposure bake at 110 °C for 1 minute.	-The method combines the possibility of fabricating sub-micron metallic gratings over large areas through pulsed LIL on a photoresist layer: 80 mm^2 areas were achieved. -r2r compatible with vacuum requirements for metal sputtering and etching. -Cost is not low: the laser source is expensive.	Selective etching is required in the dry etching hardware to achieve local processing, i.e. to remove material only in the intended grating area and not the entire exposed surface in the etching chamber.
Nano imprint (gold nano particles)	**Grating:** Gold (Au) NPs (diameter of 25 nm) separated by a MoO_3 nano-spacer (thickness from 2 nm to 70 nm) from a Silver (Ag) grating film 80 nm thick. **Substrate:** PDMS.	No adhesion promoter.	Thermal evaporation of Ag under vacuum 10^{-6} Torr. Au NPs: chemical reduction chloroauric acid with sodium citrate, boiling and stirring at room temperature for 8 h.	T_{curing} of liquid PDMS =79 °C for 3-4 h.	-The distribution of the NPs has to be uniform and compact. - R2R compatible with vacuum requirement for metal deposition.	A heterogeneous integration on polymer films is needed after fabrication of individual gratings.

Process Name	Grating / Substrate Material	Adhesion Promoter	Used Chemical & Physical Treatments	Processing Temperature	R2R Compatibility	Local Processing
Melt and Mold fabrication	**Grating:** Field's metal $L_{liquidus}$ = 62 °C, Bi/Sn, Ga, or In; Pure metals of bi- and tri-component alloys. **Substrate:** Substrateless.	Nothing.	No chemicals.	Melting temperature depending on the metal component only. With Indium T_m=157 °C and Gallium T_m < 30 °C.	- A heterogeneous transplantation is needed with organic binders or by thermal compression. The transplantation can be performed with robot arms, and the gratings can be mounted on a donor substrate in order to be transferred in a single process run. - Affordable materials favorable for low-cost fabrication.	Replica sizes are dependent from the original master and from the molds used.
Flip and Fuse	**Grating:** Metal with $T_{liquidus} \neq T_{processing}$ e.g.: chromium (Cr), copper (Cu), tin (Sn), aluminum (Al) (feature sizes ranging from 15 µm-200 µm of 1 µm thickness were successfully fabricated) **Substrate:** Flexible thermoplastics such as polyethylene terephtalate (PET), polyvinyl chloride (PVC) and polycarbonate (PC) films (175 µm).	- Polyimide non-stick coating between the silicon substrate and the metallic layer. - Pure indium (50 nm layer) and various low temperature indium-based ductile alloys. e.g. (52 w.% In 48 w.% Sn) and (97 w.% In 3 w.% Ag) with solidus temperature ≤ 157 °C to be oxidized.	Technic NI 555 at 60 °C for resist removal on the stamp. Acetone and isopropyl alcohol to remove organic residues on the stamp.	- Metallic coating and indium foundation evaporated at room temperature onto the stamp substrate. - Differential heating of the donor/receiver system: the stamp was heated at 200 °C (including the metal coating) and the receiver polymer film (PC) was heated at 145 °C.	- Low manufacturing costs by using an ultra-thin adhesion promoter and conducting the coating process at ambient conditions. - Separation step is performed by bending of the flexible substrate. - Systems of 5x5 mm^2 were achieved. Larger areas can be produced by stitching smaller area coatings.	With use of robot arms, stamps can be picked and placed where desired.

3.4 Evaluation and Results

The mentioned fabrication schemes in the previous section can be brought under three main categories, as depicted in Diagram 1.

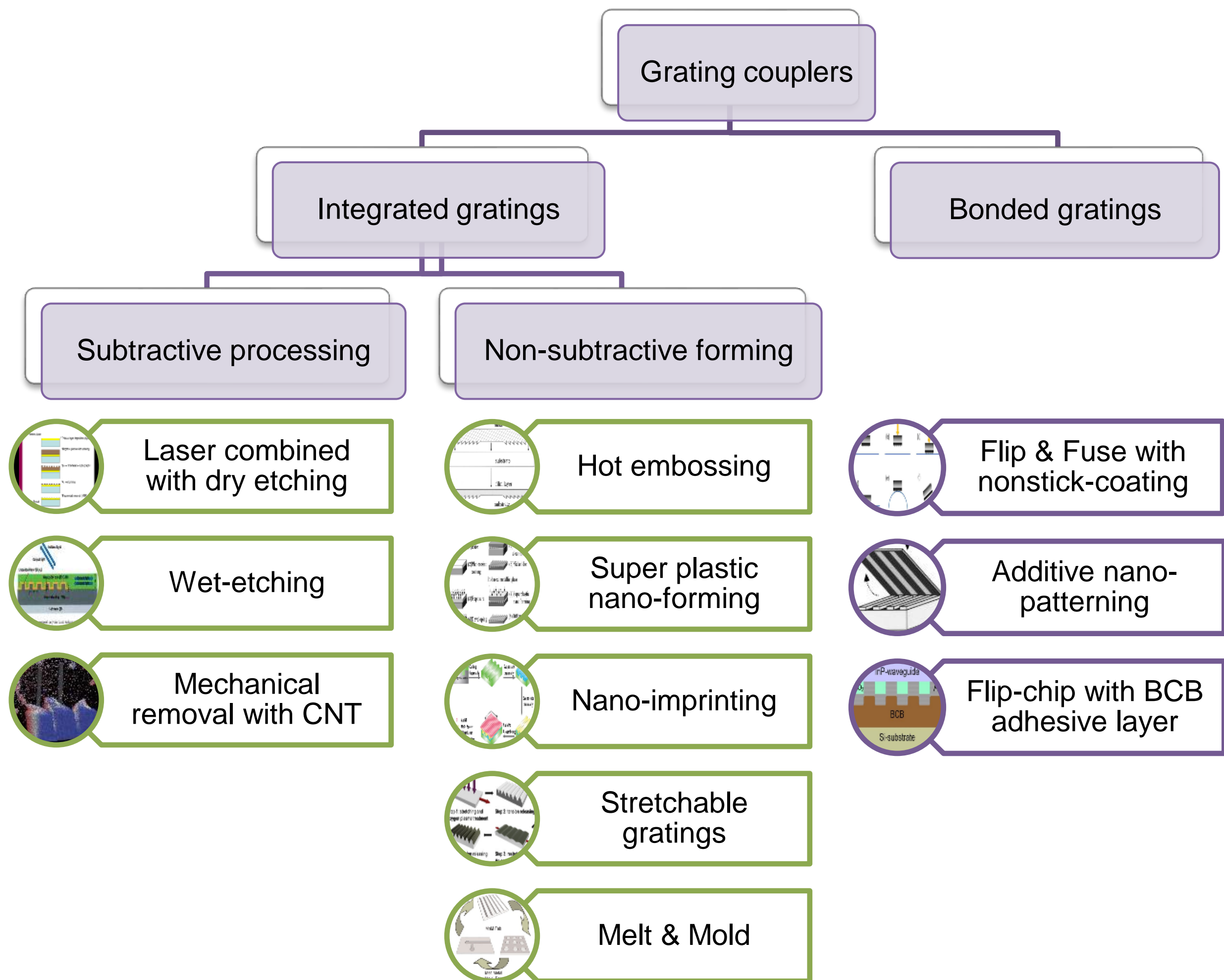

Diagram 1: State-of-the-art fabrication schemes of grating couplers

These schemes are mostly applied on rigid and thermally and chemically stable substrates, and thus, need to be adapted to the polymer material. The involved process aspects of the fabrication categories will be discussed as next.

- **Subtractive methods**

The presented subtractive methods use either aggressive chemical substances (e.g. acids) or high energy sources (e.g. ion beam), and could therefore lead to the deterioration of sensitive polymer platforms.

The conventional EBL method presents also several drawbacks. Despite its accuracy and ability to create small features, it is limited to small areas because it is very time consuming.
The laser-based technique could be customized to enable the patterning at polymer compatible temperatures. But, the complexity of the configuration of laser energy makes the technique costly and difficult to be used in mass production.
In the case of the mechanical removal with CNTs, the process is complex and very expensive. For instance, a grating with a period of 1 µm requires a density of 1000 nano tubes / mm.
In addition, subtractive processing is always coupled with material waste, which would affect the overall cost for mass production.

- **Non-subtractive forming**

Forming fabrication techniques such as molding, contact printing and embossing produce only one component of the flexible device at a time. They require either additional organic binders to join the metallic structure with the organic polymer substrate, or the application of high temperatures on both the inorganic material and receiver polymer to achieve the mechanical bond between the two components.
In addition, some of the forming techniques, such as hot embossing, would require a subsequent coating step generally under vacuum to deposit a pure metallic film. This is difficult to carry out, since polymers tend to outgas under those conditions. Coating processes require also complex and expensive systems.

- **Additive methods**

The rest of the additive fabrication methods seem to be a good alternative for the patterning of the organic substrate, since they respect the thermal and mechanical budget of the polymer.
These processes deliver either a mechanical (BCB adhesive layer) or chemical bond with the metallic component. The chemical adhesion was achieved for example by an intimate physical contact of plasma treated surfaces of both the substrate and the metal, to induce a common condensation reaction without the application of heat. The aforementioned technique successfully patterned thin layers of up to 50 nm.

Furthermore, thicker layers of up to 1 µm were fabricated by the flip and fuse technique through application of thermal-compressive loads to form hydroxyl groups on the oxidized coating/adhesion promoter and induce the adhesion mechanism.
Both of the last two techniques satisfy mass production requirements in regard to simplicity and low cost. Since the flip and fuse technique was developed mainly for flexible and temperature sensitive polymers, the next section of this thesis will focus on this novel method to study its suitability for the fabrication of grating structures.

4 Failure Mode and Effect Analysis of Procedures for the Fabrication of Metallic Gratings

4.1 Introduction

Failure mode and effect analysis (FMEA) is a methodological process that is used to discover the most serious errors of products and their manufacturing processes ahead of time in order to be able to avoid them using well-targeted countermeasures. Removing errors from the beginning ensures quality and reduces development time and cost of errors [64]. Moreover, the matter of product liability is becoming more and more important so that the quality has to be improved using all the appropriate means, such as FMEA.

The Failure Mode and Effects Analysis is nowadays one of the most important and cost-effective standard methods of preventive quality assurance. With the help of the FMEA, a qualitative risk analysis, including a detailed documentation of the potential errors and the effective action strategies can be performed [48].

The FMEA method is not only used frequently, but it also offers the greatest potential benefits compared to other quality management methods [48, 64].

4.1.1 Origin of FMEA

The FMEA method was developed in the mid 60s at NASA for quality assurance in space programs. Then, it was applied in safety-critical areas, such as aerospace and aeronautical engineering or nuclear technology. Since the mid 80s, the use of FMEA in the automotive industry has been reinforced. The American Ford Company was the first automotive company to integrate this method into its quality assurance concept. Later, the DIN EN 60812 standards were created, where the method of FMEA is described, internationally standardized and detailed [4].

4.1.2 Objectives of FMEA

The FMEA is a preventive error analysis that must be performed in an early stage of development and production phase [64]. The aim is to determine possible sources of errors and deviations and the resulting consequences for a product or a process, to prioritize and to avoid them as early as possible. Appropriate optimization measures for risk minimization are then defined and implemented.

4.1.3 Prerequisites

Important prerequisites for an effective application of the FMEA are good preparation, time planning during the product creation process and the participation of an interdisciplinary team. The progression of the FMEA should be monitored and evaluated during the project [64].

4.1.4 Legal Aspects of FMEA

The application of FMEA is not required by law, but necessary [64]. An important argument for this is the reduction of the risk of product liability claims and product recalls.

The creation of the FMEA must meet the following requirements, depending on the country and the product. In Germany, for instance, all of these requirements have to be respected in the automobile industry:

- Standards and regulations:
  - DIN EN 60812.
  - ISO / TS 16949: 2002.
  - VDA Volume 4 (Verband der Automobilindustrie).
  - AIAG FMEA (Automotive Industry Action Group).
- Customer specifications (FMEA as a contract).
- Company's specifications to ensure its goals (such as good quality, cost reduction by avoiding losses caused by defects or malfunction of the manufactured product).

4.1.5 Types of FMEA

Originally, there were three types of FMEA: System FMEA, design FMEA and process FMEA [48]. A clear separation between the system and design FMEA was in practice not possible. Therefore, the FMEA methodology is now divided to process and design FMEA, combining this way the former design FMEA with system FMEA. The designation of "design FMEA" has been reformulated to product FMEA.

4.1.5.1 Product FMEA

The design or product FMEA is used to analyze the system hardware prior to the first production run and identify any possible design-related failure modes up to the lowest part level. Corrective and preventive actions are then defined to ensure the functions of the systems, subsystems or product components over their life cycle [64].

4.1.5.2 Process FMEA

The process FMEA ensures the quality and the reliability of the process. It analyzes all manufacturing procedures and assembly processes of the product. The influencing factors of the process (such as man, method, machine, material and environment) are examined in separate process steps [64].

4.1.6 Sequence of FMEA

The process FMEA should be started when the first practical ideas are developed through the process; ideally when the product FMEA is already created. The Process FMEA is then carried out in parallel with the process planning. The VDA association has described the process model to create the FMEA details. It consists of five phases, which are shown in Figure 46 [47].

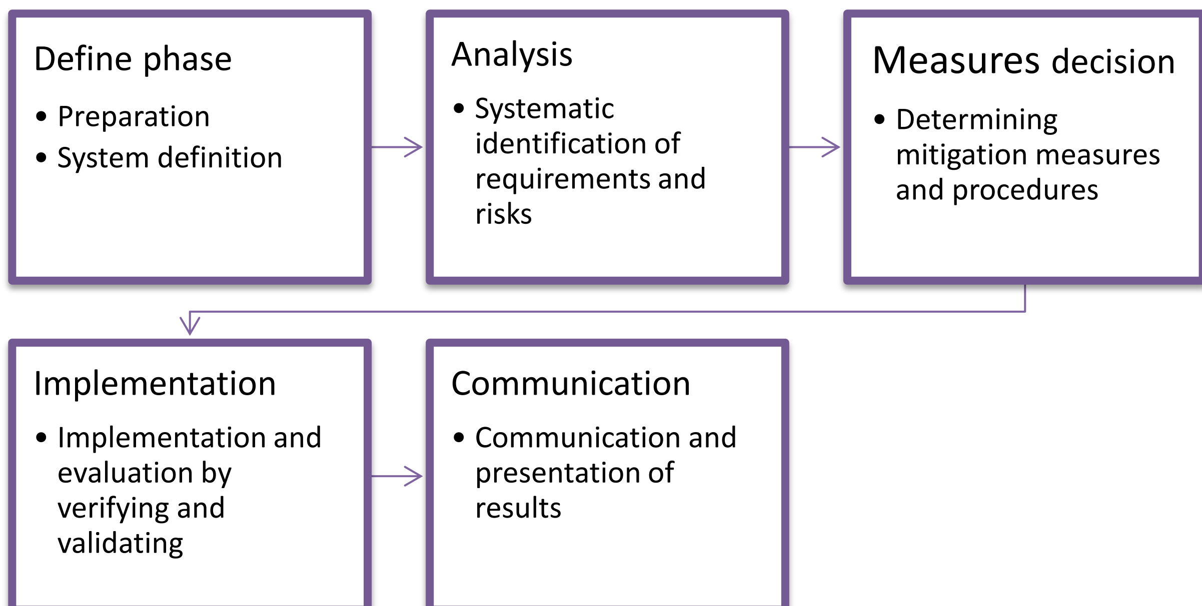

Figure 46: The DAMUK© model for the FMEA creation.

4.1.7 Limitations of FMEA

FMEA is a well structured risk assessment approach with a high efficiency in detecting breakdowns in products or functions. However, the methodology has some limitations and weaknesses. It may, for instance, not be able to cover all the failure modes of a system because of its complexity, or the limitations of knowledge of the team [64]. The scoring is also very subjective, and minor variations (from score 2 to 1, for example), will result in a significantly higher risk priority number (RPN), since it is the multiplication output of all sub- scores [4].

4.1.8 The FMEA Procedure

In order to conduct an FMEA on a desired process, it should be proceeded according to the steps depicted in Figure 47 and described in the following paragraphs [4, 48, 64]:

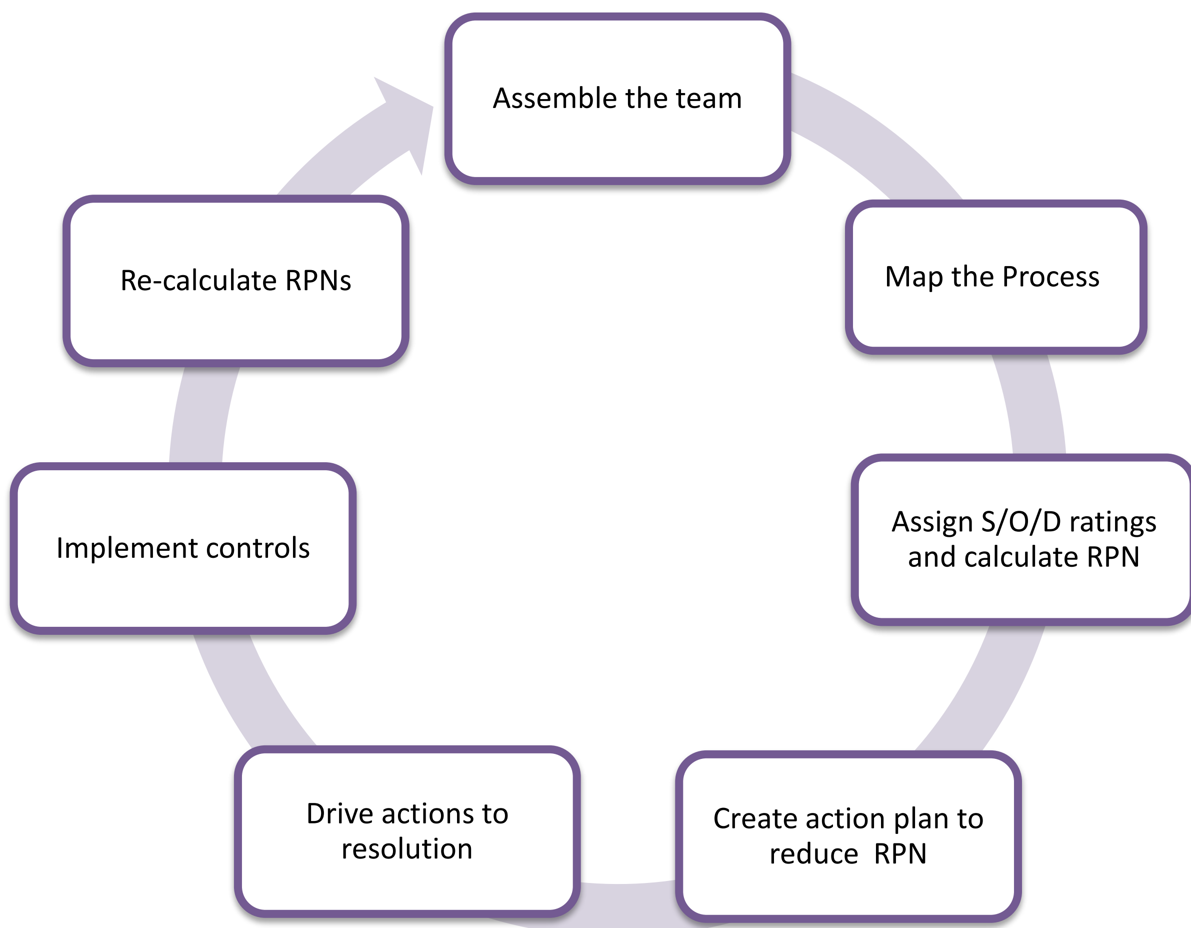

Figure 47: FMEA flow cycle. S, O and D are the Severity number, the Occurrence number and the Detectability number, respectively. RPN is the Risk Priority Number.

Step 1: Reviewing the process components and its functions

The reviewing of the process in a detailed flowchart helps the FMEA team to become familiar with the process and have a visual reference for the entire FMEA cycle. It helps also identify and determine all the components and functions of the process.

Step 2: Brainstorming of potential failure modes

The execution of an FMEA is done within an FMEA team [4], which consists of all operational areas of concern in the analysis. The execution of the FMEA is performed under the direction of an FMEA moderator, which has the quality of mastering the methodology of the procedure, and ensures this way a smooth analysis conduction without wasting time in discussions concerning the method. While the moderator gives methodical knowledge, the rest of the team brings in technical knowledge concerning the product or process to be analyzed [4]. A potential failure mode represents any way in which the component or process step could fail to perform its expected functions. To guarantee a successful FMEA, supervisors are imperative to assist the FMEA actions, “the moderator has to provide good methodical and moderating knowledge and the team has to be a small, success-oriented team consisting out of involved members closely associated with the product” [4].

Step 3: Defining of potential effects of failure

Potential effects are the impacts caused by a potential failure on the performance of a product or a system. They should be specifically defined in order to identify actual potential risks.

Step 4: Assigning ranking scores to the identified effects

For this step, it is imperative for the team to agree on the ranking criteria and use them consistently throughout the organization for different FMEAs.

- **Severity (S):** The severity ranking is based on a relative estimation of how serious an effect would be if it occurs. It can be assigned from a low (1) to a high (10).

- **Occurrence (O):** The occurrence ranking is scored in the same manner as severity. It is based on how frequently the failure mode would occur. Hence, the knowledge of the failure cause, also called mechanism, is very helpful.
- **Detection (D):** Detection is scored in reverse with respect to severity and occurrence. The ranking scale (1) means the failure is certainly detectable and (10) means absolutely undetectable.

Detection rankings are assigned to each process or product control already available to detect the specific mode of failure.

Step 5: Calculating the Risk Priority Number (RPN)

The RPN is calculated for each failure mode and effect by multiplying the three rankings together RPN=SxOxD. The RPN gives a relative risk ranking to prioritize improvement targets. As a start, the team can initially focus its attention on the failures with the highest 20% of the RPN scores.

Step 6: Developing the action plan to reduce the RPN

The RPN can be reduced by lowering any of the three rankings (S, O, or D) individually or in combination with one another.
S can be reduced by physically modifying the process equipment or layout.
O can be reduced by removing or controlling the potential causes.
D can be reduced by improving the process controls in place.

Step 7: Taking corrective and preventive actions

The action plan defines what steps are needed to be implemented in the solution, who will do them, and when they will be completed.

Step 8: Recalculating the resulting RPN

This step in an FMEA enables the team to determine the effectiveness of the corrective and preventive measures taken. After the completion of the action plan, a second cycle of risk assessment for the failure modes can be conducted to recalculate the new RPN. A successful FMEA should come out with lower RPNs.

4.2 Process-FMEA Application on the Flip and Fuse Technique

In this section, the three main processing sequences of F&F (Stamp fabrication, Flip & Fuse and Separation by centric bending) will be analyzed according to the previously described 1-8 steps of the process FMEA.

Some basic assumptions are made to exclude failure modes that can be avoided with improved process controls. Therefore steps 4 to 6 are not applicable any more. The following items, for example, have been discarded from the analysis:

- Environmental impurities (dust, humidity…)
- Irregularities or failure of the diffusion mechanism caused, for example, by an insufficient contact time between the donor and the receiver, a partial coverage of the heat/pressure affected zone with the processing tool, a non-uniform temperature distribution or shrinkage and expansion mismatch due to discrepancies in the thermal expansion coefficients between the metal stack and the polymer film, a non-uniform formation of the oxide layer on the metal surface, etc…
- Robot malfunctioning in positioning the fabricated chips, resulting in alignment/tilt inaccuracy.
- Lack of sensor equipment needed for failure detection of any art.
- Deficiencies of the mass production machinery modules, setups or configurations, such as misalignment of the polymer foil under the process module.

The next paragraphs are devoted to the detailed analysis of each processing sequence of F&F technique.

4.2.1 Sequence 1: Stamp Fabrication

Step 1: Definition

The fabrication of the metallic grating on the rigid stamp takes place in a class 100 clean room at 20°C and 50% relative humidity. The developed approach consists in coating a double side polished silicon substrate with a non-stick layer of polyimide (PI) and then depositing the desired metallic material to realize the grating component. The adhesion foundation is then placed on top of the metallic bundle and

the end product is cleaned and diced for further processing. The following illustration shows an example of the resulting silicon stamp with metallic strips:

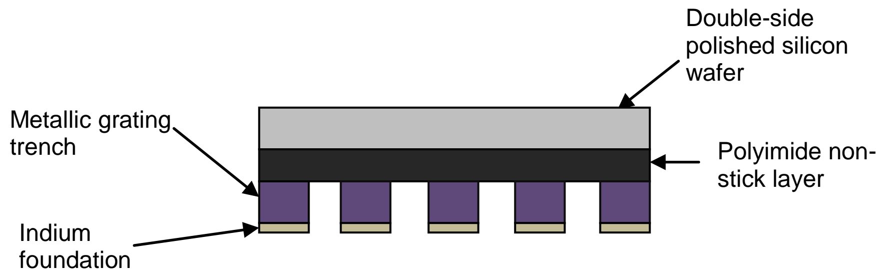

Figure 48: Schematic illustration of a rectangular grating pattern on the donor stamp.

Step 2, 3 and 7: Potential failure modes, explanation and countermeasures

At this stage of the procedure four difficulties might be encountered:

1) Mirroring

This is an inherent limitation of the process, which consists in inverting the layers order of appearance in the metallic stack once transferred to the receiver substrate; as depicted in Figure 49.

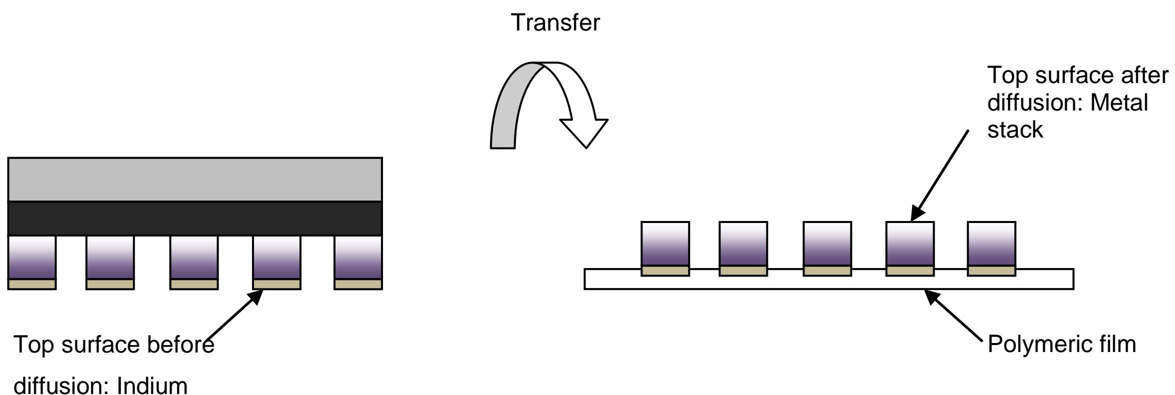

Figure 49: Structures/ Layer order on the stamp (left) and on the receiver after transfer (right).

As a counter measure, the order of the deposited metallic layers should be considered during the design phase.

2) Planarity of the top grating surface

In the case of pointy grating shapes (sinusoidal, triangular, etc.), deposited on a planar PI layer, significant shape changes can occur at the tip. Under the application of pressure, material displacement can happen in the free space between the shape

peaks, because there is no supporting material. This leads to high geometrical inaccuracies as depicted in Figure 50.

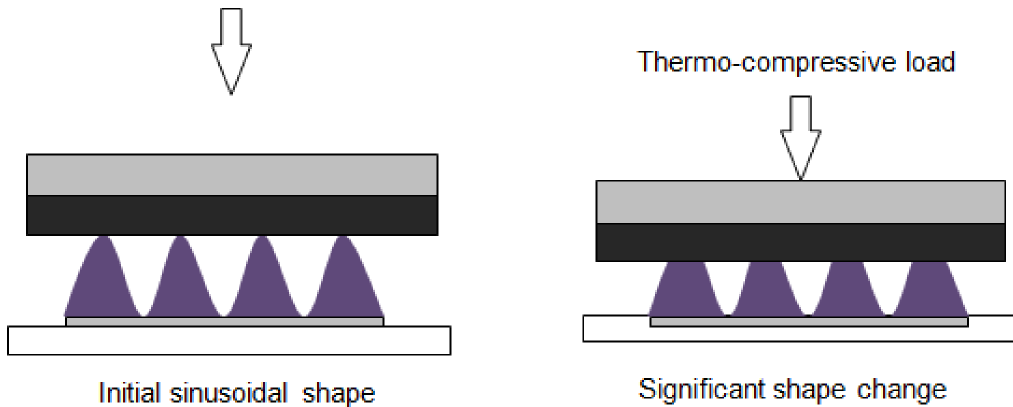

Figure 50: Schematic illustration of shape modification in an example of sinusoidal grating before (left) and after (right) load application

The realization of the pattern in this case can be solved through the modification of the polyimide coating shape, from the regular planar surface to a negative master mold of the corresponding grating grooves (Figure 51).

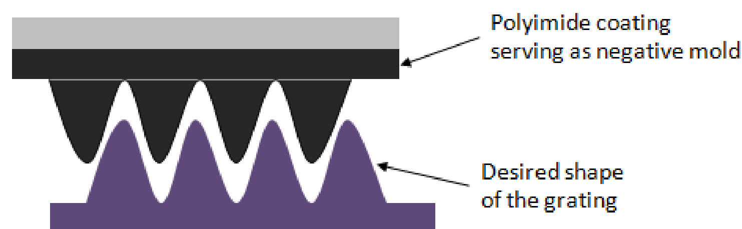

Figure 51: Pre-molding of the polyimide coating to fit in the shape of the metallic grating.

The transfer of the shapes from the non-planar polyimide molds to the polymer film is discussed in the next paragraph and countermeasures are given.

3) Interlocking

It is very important to consider the separation step in the design at this early stage to ensure the morphological stability of the metallic material once uncoupled from the rigid donor stamp. For example, in the case of a conventional rectangular grating (see Figure 52), a failure might occur when separating the pattern from the negative master. The joint between the two materials may not be released without possible

damage of the upper surface and the groove edges of the grating (highlighted in continuous red line on Figure 52) once performing the separation by bending.

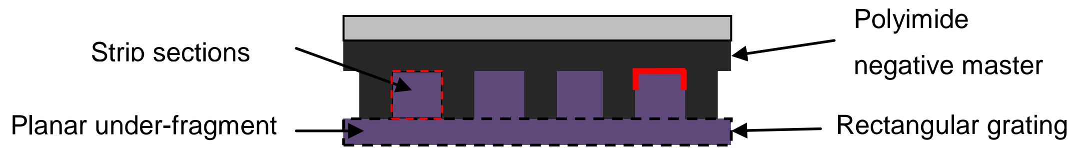

Figure 52: Fabrication model of a rectangular grating with a PI negative mold.

In this case, an extra patterning-fusion-and-bending step is required for the shape formation (Figure 53). This solution begins with the fabrication of the continuous planar under-fragment of the grating according to the regular F&F process, outlined in black dashes in Figure 52, then adding the strip sections on top of the resulting polymer-metal compound with a second F&F processing step.

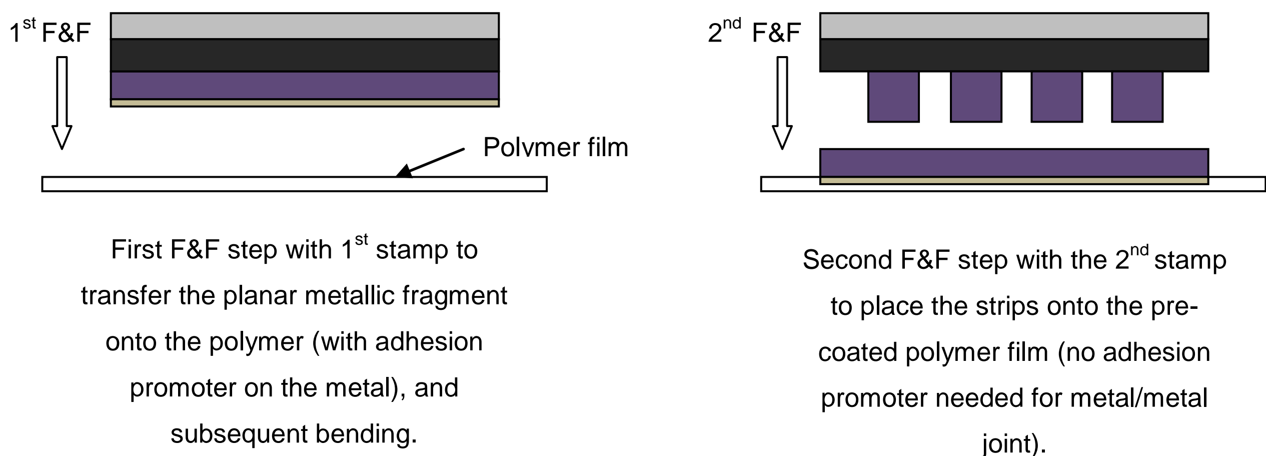

Figure 53: Two-step F&F processing.

4) Strong chemical bond between the thermosetting PI and the metal

The fourth failure mode would be when the grating material holds too tight to the polyimide coating at their interface. This is explained by the diffusion of the metal in the thermosetting compound, PI, and results later either in pattern transfer inhomogeneities or in the total failure of the separation. In the former case, this might be caused when the strength of the joint between the receiver polymer and the oxidized metal is higher than the joint strength of the PI/metal system.

Thus, separation takes place within the metal with a roughened outer surface (se Figure 54).

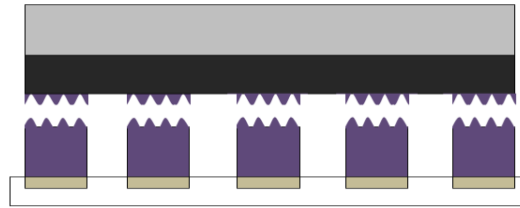

Figure 54: Roughened surface after separation.

In the latter case, the failure of the decoupling is generated when the bond magnitude between the flexible polymer and the metal is insufficient for breaking the bond in the rigid polymer (PI)/metal joint.

For instance, the presence of the adhesion promoter (Figure 55) in the polyimide coating may lead to the formation of a strong chemical bond between the PI and some inorganic surfaces, such as copper, aluminum, silicon nitride [11].

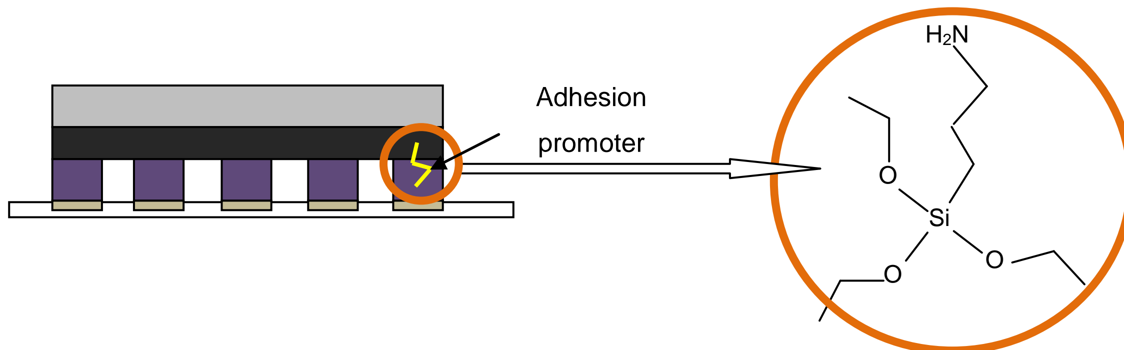

Figure 55: 3-Aminopropyltriethoxysilane embedded in the organic material PI to promote adhesion to the inorganic substrate.

It is also to be noted that adhesion of polyimide deposited on a metal is different than adhesion of a metal deposited on cured polyimide [24]. The first constellation tends to lead to a stronger adhesion than the second [15]. In the case of the F&F process where the metal is deposited on the polyimide, the final bond strength is strongly determined by the nature of the metal; The inorganic material can either react with the PI and form an interfacial connection, such as chromium, or can diffuse in the polymer and form metal clusters in the vicinity of the interface, as in the case of copper and nickel [17, 28]. In [15], copper and aluminum were shown to diffuse into the polyimide at room temperature. Whereas chromium might interpenetrate the polymer upon heating and a very thin interlayer of titanium may prevent an unwanted diffusion of the copper material.

As a summary, the choice of the metal (with regard to its reactive ends) and/or the polyimide (with regard to embedded adhesion promoter) should be considered to avoid a possible diffusion mechanism between the two involved system components.

4.2.2 Sequence 2: Flip & Fuse

Step1: Definition

After the stamp preparation, the Fuse process step of the grating is conducted at ambient conditions. It uses only a thermo-compression load applied by a commercial flip chip bonding tool to assemble the metallic patterns with the polymer film (see Figure 56). Essential procedure parameters, such as heating/cooling rates and timing are given in [1] to ensure the success of the diffusion.

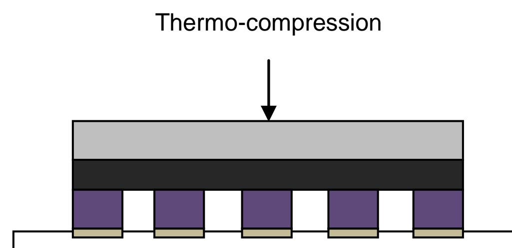

Figure 56: Schematic illustration of the thermo-compressive load of the bonding tool for the pattern transfer.

Step 2, 3 and 7: Potential failure modes, explanation and countermeasures

The pressure and heat combination used for bonding might cause enlargement and flattening of the grating pattern once transferred (see Figure 57). The gravity of the deformation is mainly dependent on the mechanical behavior of the metallic material (ductile/brittle). This failure mode might induce dimension infidelities from the original design (i.e. width, height and depth). It could also result in morphology instability with ductile materials or detrimental damage of the grating with more brittle materials in regard to shape, structure or surface topography.

Some of these parameters (such as the grating period, the groove depth or the filling factor) are considered in the diffraction equation presented in 2.3.4.2, and thus, this failure might affect the optical coupling properties of the grating, such as the diffraction modes.

The flattening of the groove shape is an inevitable artifact of F&F due to the use of the thermo-compressive force to achieve the diffusion between the functional metallic layer and the polymeric receiver. The morphology of the grating gets damaged, resulting in wider, shallower and less spaced slits/corrugations. Figure 57 gives an example on a rectangular grating.

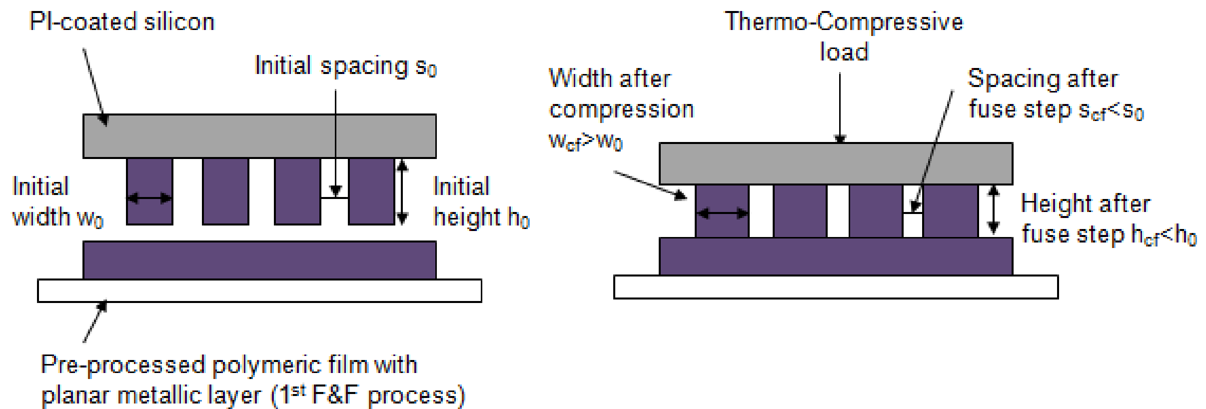

Figure 57: Grating geometrical parameters: (left) before, (right) after fusion step.

A simple design adjustment for the stamp fabrication prior to the fuse conduction may remedy to this inherent process outcome.

4.2.3 Sequence 3: Separating by Bending

Step 1: Definition

After the saturation of the diffusive bond between the metal oxide and the polymer film, the separation is conducted by centric bending on a cylinder with a prefixed radius in order to implement the novel F&F procedure in a roll-to-roll manufacturing method (see Figure 58).

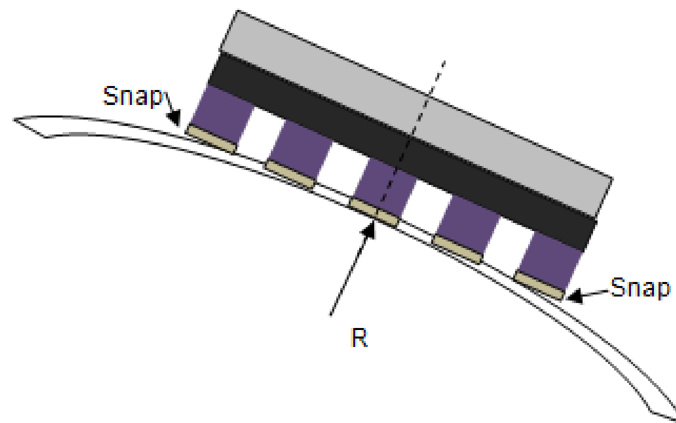

Figure 58: Bending for separation of the rigid stamp and the polymer film.

Step 2, 3 and 7: Potential failure modes, explanation and countermeasures

At this stage, the morphology of the grating (shape, structure or surface) might be damaged while bending due to the mechanical limitations of the metal material or the wrong choice of the radius of curvature for the bending of large surface area and thin structures. The mechanical limitations can be explained either by the softness or the brittleness of the inorganic compound. Brittle materials absorb little energy and fail at low strains, while ductile materials have a greater fracture energy [50].

If the metal is too soft, the bending might cause the deformation of the original shape, such as straining the side edges and the surface. If the metal is too brittle, early quick micro-cracks and crack propagation on the free surfaces might be encountered (see Figure 59).

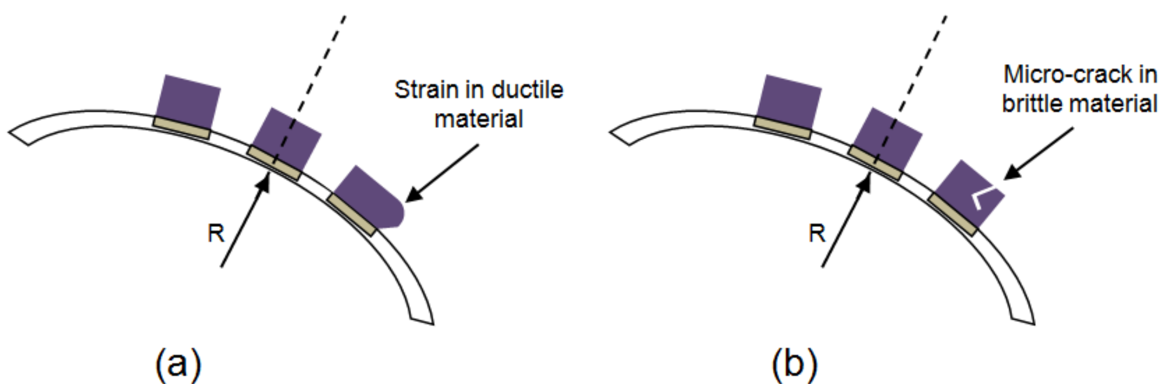

Figure 59: (a) Strain after bending of ductile material, (b) Micro-crack after bending of brittle material

To mitigate these potential failure modes, a good choice of the metal and/or the adjustment of the radius of curvature are imperative.

The stress-strain curve (Figure 60) of a selected metal has to be used to give a prediction of possible structure damage. A substantial geometrical deformation, i.e. a permanent plastic deformation of the grating, due to a mechanical stress applied above the yield point might cause a serious irreversible failure mode to the performance of the metallic component.

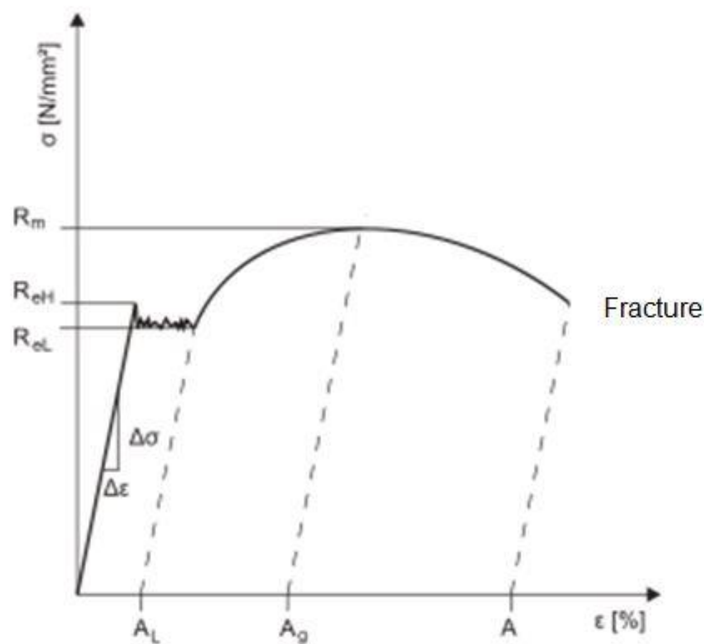

Figure 60: Stress-strain curve for ductile materials [35].

The investigated material exhibits an elastic behavior when the applied stress does not exceed the yield strength. The elasticity is defined by the ability of the object to resist the stress and to restore its former size and shape when the force is removed.

With dimensions decreasing, morphology issues of metallic layers under bending are aggravated as reported in [30], resulting in the rupture of the metal thin film at small tensile strains (often between 1-2 %). Nevertheless, the metal material could stand larger tensile strains when supported by a polymer film, because the substrate helps retarding the strain localization [34]. It was also found in [67] that the interfacial strength plays an important role; the better the bond between these two material compounds, the larger is the stress sustainability of the metal.

Based on the study in [30], the maximum tensile strain without plastic deformation of the metal film of choice can be defined as:

$\varepsilon_{yield} = \frac{(d-t)}{2R}$, where:

d is the thickness of the polymer substrate

t is the thickness of the metal film

R is the substrate curvature radius, which is the bending radius of the rolling cylinder in F&F, and can be determined through the geometrical relationship: $R = \frac{\ell^2+\delta^2}{2\delta}$, where ℓ is the half of the span length (which is half of the width of the donor stamp in F&F) and δ is the displacement of the loading tip (in F&F the load is applied by means of a Flip Chip bonding tool).

If the tensile stress corresponding to a certain tensile strain does not reach the yield stress of the metal film (with a certain thickness), then no cracks are expected to appear.

5 Conclusion

In this thesis, the state of the art in metallic grating fabrication on thin polymer sheets was researched and summarized in order to provide recommendations for use in micro optical grating couplers production within PlanOS research project.
First, the state of the art in polymer films technology was presented with details about the most influencing parameters that affect its processability and suitability for mass production.
Adhesion between organic and inorganic materials was found to be a main challenge in the processing of metallic gratings on polymers. So, it was explained in detail, and solutions were provided from literature.
Then, the state of the art in fabrication schemes for gratings was investigated. Several processes were determined, and the need of a proper categorization arose since many fabrication schemes shared similarities or were slightly adapted or optimized for different uses. This led to the setup of three main processing categories.
Regarding the applicability on flexible substrates, most of the fabrication techniques which are well known and established were found to be used on rigid substrates and temperature enduring materials, yet not with low temperature polymers. Some other processes are innovative and could also be used for the polymers of interest.
An overview matrix of selected fabrication schemes presenting the most important process parameters and giving hints about roll-to-roll compatibility and possibility of local processing was developed to help during the selection of a proper process for micro metallic gratings on polymers.
A decision to investigate further the Flip and Fuse (F&F) technique was taken, since it presented the highest potential. This method was developed at the IMPT and consists in the coating of metallic materials on polymer substrates with low transition temperatures. It is performed at ambient conditions and the diffusive mechanism between the two substrate materials is achieved by means of a thermo-compressive energy and an implemented adhesion promoter on top of the metallic layer stack.
Finally, a Failure Mode and Effect Analysis (FMEA) was conducted for the chosen process. The main failure modes consist of:

- Mirroring issues by inverting the layers order of appearance in the metallic stack once transferred to the receiver substrate.
- Planarity of the top grating surface leading to shape changes at the tip of pointy grating shapes (sinusoidal, triangular, etc.).
- Interlocking during stamp fabrication, resulting in morphological changes of the metallic material once uncoupled from the rigid donor stamp.
- Strong chemical bond between the polyimide and the metal, causing roughened surfaces after separation.
- Enlargement and flattening of the grating pattern once transferred to the polymer due to the pressure and heat combination used for bonding.
- Morphology damages of the grating while bending due to the mechanical limitations of the metal material or the wrong choice of the radius of curvature for the bending.

At the end, countermeasures were suggested for all the mentioned failure modes. Further steps after this work would be to carry out practical experiments with the F&F method to produce metallic grating structures on thin polymer films taking into consideration the recommendations from the conducted FMEA.

References

[1] Akin, M., Brokbals, V., and Rissing, L. 2016. Flip and Fuse: A New Technique for Diffusive Coating of Organic, Flexible, and Low-Transition-Temperature Substrates With Inorganic Materials in Roll-to-Roll Processes at Ambient Conditions. IEEE Transactions on Components, Packaging and Manufacturing Technology 6, 8, 1276–1282.

[2] Arriola, A., Rodriguez, A., Perez, N., Tavera, T., Withford, M. J., Fuerbach, A., and Olaizola, S. M. 2012. Fabrication of high quality sub-micron Au gratings over large areas with pulsed laser interference lithography for SPR sensors. Opt. Mater. Express 2, 11, 1571.

[3] Bargel, H.-J. and Schulze, G. 2012. Werkstoffkunde. Springer Berlin Heidelberg, Berlin, Heidelberg.

[4] Bertsche, B. 2008. FMEA – Failure Mode and Effects Analysis. Springer Berlin Heidelberg.

[5] Bicerano, J. 2002. Prediction of Polymer Properties. CRC Press.

[6] Bonod, N. and Neauport, J. 2016. Diffraction gratings: from principles to applications in high-intensity lasers. Adv. Opt. Photon., AOP 8, 1, 156–199.

[7] Brédas, J. L. and Chance, R. R. 2012. Conjugated Polymeric Materials: Opportunities in Electronics, Optoelectronics, and Molecular Electronics. Springer Netherlands.

[8] Cheng, M.-C. and Sung, C.-K. 2011. Fabrication sub-10nm metallic gratings with carbon nanotube - A study by molecular dynamics simulation method. IEEE.

[9] Colinge, J.-P. 2004. Basics of Silicon-on-Insulator (SOI) Technology. Springer Berlin Heidelberg.

[10] Domininghaus, H., Elsner, P., Eyerer, P., and Hirth, T. 2012. Kunststoffe. Eigenschaften und Anwendungen ; mit 275 Tabellen. VDI-Buch. Springer, Heidelberg u.a.

[11] 2015, Hanover. Fujifilm Electronic Materials. Polyimide-Workshop at Institue of Microproduction Technology (Apr. 2015, Hanover).

[12] G. RAMARATHNAM, M. LIBERTUCCI, M. M. SADOWSKI and T. H. NORT. 1992. Joining of Polymers to Metal. The joining of high-strength thermoplastics to

aluminum is one phase of an ongoing study of polymer-to-metal joints. WELDING RESEARCH SUPPLEMENT (Dec. 1992).

[13] Gausemeier, J. and Bigl, T. 2006. Integrative Entwicklung räumlicher elektronischer Baugruppen. Hanser, München.

[14] Gent, A. N. and Hamed, G. R. 1990. Fundamentals of Adhesion. Springer US.

[15] Ghosh, M. 1996. Polyimides: Fundamentals and Applications. Taylor & Francis.

[16] Gou, Y. and Xuan, Y. 2013. The application of the microstructured metallic grating to light emission extraction. Chin. Sci. Bull. 58, 6, 696–700.

[17] Gupta, D. 2013. Diffusion Processes in Advanced Technological Materials. Elsevier Science.

[18] Harper, K. 2003. Theory, Design, and Fabrication of Diffractive Grating Coupler for Slab Waveguide. All Theses and Dissertations.

[19] Higuera-Rodriguez, A., Dolores-Calzadilla, V., Jiao, Y., Geluk, E. J., Heiss, D., and Smit, M. K. 2015. Realization of efficient metal grating couplers for membrane-based integrated photonics. Optics Letters 40, 12, 2755–2757.

[20] Hilleringmann, U. 2014. Lithografie. Springer Fachmedien Wiesbaden.

[21] Hösel, M. 2013. Large-scale roll-to-roll fabrication of organic solar cells for energy production. PhD thesis. DTU Energy Conversion and Storage, Roskilde.

[22] Hösel, M., Søndergaard, R. R., Jørgensen, M., and Krebs, F. C. 2013. Fast Inline Roll-to-Roll Printing for Indium-Tin-Oxide-Free Polymer Solar Cells Using Automatic Registration. Energy Technology 1, 1, 102–107.

[23] Joram, C. 2009. Transmission curves of plexiglass (PMMA) and optical grease PH-EP-Tech-Note-2009-003.

[24] Kim, Y.-H., Walker, G. F., Kim, J., and Park, J. 1987. Adhesion and interface studies between copper and polyimide. Journal of Adhesion Science and Technology 1, 1, 331–339.

[25] Kisin, S., van der Varst, P., and With, G. de. 2007. Adhesion and adhesion changes at the copper metal–(acrylonitrile–butadiene–styrene) polymer interface. Thin Solid Films 515, 17, 6853–6859.

[26] Koltzenburg, S., Maskos, M., and Nuyken, O. 2014. Polymere: Synthese, Eigenschaften und Anwendungen. Springer Berlin Heidelberg, Berlin, Heidelberg.

[27] Kooy, N., Mohamed, K., Pin, L. T., and Guan, O. S. 2014. A review of roll-to-roll nanoimprint lithography. Nanoscale Research Letters 9, 1, 320.

[28] LeGoues, F. K., Silverman, B. D., and Ho, P. S. 1988. The microstructure of metal–polyimide interfaces. Journal of Vacuum Science & Technology A 6, 4, 2200–2204.

[29] Lekishvili, N. G., Nadareishvili, L. I., Vygodsky, J. S., and Samsonya, S. A. 2002. Polymers and Polymeric Materials for Fiber and Gradient Optics. Taylor & Francis.

[30] Li, Y., Wang, X.-S., and Meng, X.-K. 2008. Buckling behavior of metal film/substrate structure under pure bending. Appl. Phys. Lett. 92, 13, 131902.

[31] Li, Z., Tevis, I. D., Oyola-Reynoso, S., Newcomb, L. B., Halbertsma-Black, J., Bloch, J.-F., and Thuo, M. 2015. Melt-and-mold fabrication (MnM-Fab) of reconfigurable low-cost devices for use in resource-limited settings. Low Cost Devices for Point-of-Care, Food, and Environmental Analysis 145, 20–28.

[32] Loewen, E. G. and Popov, E. 1997. Diffraction gratings and applications. Optical engineering 58. Dekker, New York, NY.

[33] Loo, Y.-L., Willett, R. L., Baldwin, K. W., and Rogers, J. A. 2002. Additive, nanoscale patterning of metal films with a stamp and a surface chemistry mediated transfer process: Applications in plastic electronics. Applied Physics Letters 81, 3, 562–564.

[34] Lu, N., Wang, X., Suo, Z., and Vlassak, J. 2007. Metal films on polymer substrates stretched beyond 50%. Appl. Phys. Lett. 91, 22, 221909.

[35] Macherauch, E., Zoch, H.-W., and Tinscher, R. 2014. Praktikum in Werkstoffkunde. 95 ausführliche Versuche aus wichtigen Gebieten der Werkstofftechnik. Lehrbuch. Springer Vieweg, Wiesbaden.

[36] Magdenko, L., Gaucher, F., Aassime, A., Vanwolleghem, M., Lecoeur, P., and Dagens, B. 2009. Sputtered metal lift-off for grating fabrication on InP based optical devices 86, 11, 2251–2254.

[37] März, R. and Wächter, C. 2012. Integrated Optics. Springer Berlin Heidelberg.

[38] März, R. and Wächter, C. 2012. Integrated Optics. In Springer handbook of lasers and optics, F. Trager, Ed. Springer, Berlin, New York, 1209–1253. DOI=10.1007/978-3-642-19409-2_15.

[39] Maystre, D. 2012. Diffraction gratings. Scholarpedia 7, 6, 11403.
[40] Mittal, K. L. 1976. Adhesion Measurement of Thin Films. ElectroComponent Science and Technology 3, 1, 21–42.
[41] Mittal, K. L. 1976. Adhesion Measurement of Thin Films. ElectroComponent Science and Technology 3, 1, 21–42.
[42] Moazzez, B., O'Brien, S. M., and Merschrod S., E. F. 2013. Improved Adhesion of Gold Thin Films Evaporated on Polymer Resin: Applications for Sensing Surfaces and MEMS. Sensors 13, 6, 7021–7032.
[43] Musa, S. M. 2013. Computational Nanophotonics: Modeling and Applications. Taylor & Francis.
[44] Nikolova, D. 2005. Charakterisierung und Modifizierung der Grenzflächen im Polymer-Metall-Verbund, Halle (Saale), Univ., Diss., 2005.
[45] Nikolova, D. 2005. Diss Charakterisierung und Modifizierung der Grenzflächen im Polymer-Metall-Verbund.
[46] Oriol Gili, d. V. 2010. M Thesis: Design and Simulation of Vertical Grating Coupler for Photonic Integrated System-in-Package Berlin, April 2010.
[47] Pfeufer, H.-J. 2015. FMEA - Fehler-Möglichkeits- und Einfluss-Analyse. Pocket Power 64. Hanser, München.
[48] 2003. Qualitätsmanagement für Ingenieure. VDI-Buch. Springer Berlin Heidelberg, Berlin, Heidelberg.
[49] Ravve, A. 2012. Physical Properties and Physical Chemistry of Polymers. Springer New York.
[50] Rösler, J., Bäker, M., and Harders, H. 2007. Mechanical behaviour of engineering materials: metals, ceramics, polymers, and composites. Springer.
[51] Rösler, J., Harders, H., and Bäker, M. 2007. Mechanical behaviour of engineering materials. Metals, ceramics, polymers, and composites. Springer, Berlin, New York.
[52] Saotome, Y., Fukuda, Y., Yamaguchi, I., and Inoue, A. 2007. Superplastic nanoforming of optical components of Pt-based metallic glass. Proceedings of the 12th International Symposium on Metastable and Nano-Materials (ISMANAM-2005)Proceedings of the 12th International Symposium on Metastable and Nanomaterials (ISMANAM-2005) 434–435, 97–101.

[53] Schröder, B. 2014. Kunststoffe für Ingenieure. Springer Fachmedien Wiesbaden, Wiesbaden.

[54] Schwartz, E. 2006. Roll to Roll Processing for Flexible Electronics. MSE 542: Flexible Electronics.

[55] SFB/TRR 123. PlanOS Concept.

[56] Subbaraman, H., Lin, X., Ling, T., Guo, L. J., and Chen, R. T. 2014. Towards roll-to-roll manufacturing of polymer photonic devices. In SPIE OPTO. SPIE Proceedings. SPIE, 899116. DOI=10.1117/12.2044229.

[57] Sun, X., Li, J., and Hokansson, A. 2007. Study of optical fiber damage under tight bend with high optical power at 2140 nm. In Biomedical Optics (BiOS) 2007. International Society for Optics and Photonics, 643309-643309-8. DOI=10.1117/12.699202.

[58] Taillaert, D., van Laere, F., Ayre, M., Bogaerts, W., van Thourhout, D., Bienstman, P., and Baets, R. 2006. Grating Couplers for Coupling between Optical Fibers and Nanophotonic Waveguides. Jpn. J. Appl. Phys. 45, 8R, 6071.

[59] Taillaert, D., van Laere, F., Ayre, M., Bogaerts, W., van Thourhout, D., Bienstman, P., and Baets, R. 2006. Grating Couplers for Coupling between Optical Fibers and Nanophotonic Waveguides. Jpn. J. Appl. Phys. 45, 8R, 6071.

[60] Waldhäusl, R., Schnabel, B., Dannberg, P., Kley, E.-B., Bräuer, A., and Karthe, W. 1997. Efficient Coupling into Polymer Waveguides by Gratings. Appl. Opt., AO 36, 36, 9383–9390.

[61] Waldhäusl, R., Schnabel, B., Dannberg, P., Kley, E.-B., Bräuer, A., and Karthe, W. 1997. Efficient Coupling into Polymer Waveguides by Gratings. Appl. Opt., AO 36, 36, 9383–9390.

[62] Wang, L., Li, Y., Porcel, M. G., Vermeulen, D., Han, X., Wang, J., Jian, X., Baets, R., Zhao, M., and Morthier, G. 2012. A polymer-based surface grating coupler with an embedded Si3N4 layer. Journal of Applied Physics 111, 11, 114507.

[63] Weißbach, W., Dahms, M., and Jaroschek, C. 2015. Werkstoffkunde. Springer Fachmedien Wiesbaden, Wiesbaden.

[64] Werdich, M. 2012. FMEA - Einführung und Moderation. Durch systematische Entwicklung zur übersichtlichen Risikominimierung (inkl. Methoden im Umfeld). Vieweg+Teubner Verlag, Wiesbaden.

[65] Wolf, R. A. 2010. Primary Polymer Adhesion Issues with Inks, Coatings, and Adhesives. In Plastic surface modification. Surface treatment and adhesion, R. A. Wolf, Ed. Hanser, München, 3–12. DOI=10.3139/9783446430648.002.

[66] Wong, W. S. and Salleo, A. 2009. Flexible Electronics 11. Springer US, Boston, MA.

[67] Xiang, Y., Li, T., Suo, Z., and Vlassak, J. J. 2005. High ductility of a metal film adherent on a polymer substrate 87, 16, 161910-161910-3.

[68] Yin, D., Feng, J., Ma, R., Zhang, X.-L., Liu, Y.-F., Yang, T., and Sun, H.-B. 2015. Stability Improved Stretchable Metallic Gratings With Tunable Grating Period in Submicron Scale. Journal of Lightwave Technology 33, 15, 3327–3331.

[69] Ying Zhou, Xuanhua Li, Xingang Ren, Liangbao Yang, and Jinhuai Liu. 2014. Designing and fabricating double resonance substrate with metallic nanoparticles–metallic grating coupling system for highly intensified surface-enhanced Raman spectroscopy. Analyst 139, 19, 4799–4805.

[70] Ziemann, O., Krauser, J., Zamzow, P. E., and Daum, W. 2013. POF - Polymer Optical Fibers for Data Communication. Springer Berlin Heidelberg.